Journal of Medicinal Chemistry

Article

The Discovery and Characterization of the #-Amino-3-hydroxy-5-methyl-4-isoxazolepropionic acid (AMPA) Receptor Potentiator *N*-{(3*S*,4*S*)-4-[4-(5-cyano-2-thienyl)phenoxy]tetrahydrofuran-3-yl}propane-2-sulfonamide (PF-04958242)

Christopher L. Shaffer, Nandini C. Patel, Jacob Bradley Schwarz, Renato J Scialis, Yunjing Wei, Xinjun J Hou, Longfei Xie, Kapil Karki, Dianne Bryce, Sarah M Osgood, William E. Hoffmann, John T Lazzaro, Cheng Chang, Dina F McGinnis, Susan M Lotarski, Jianhua Liu, Ronald Obach, Mark L Weber, Laigao M Chen, Kenneth R Zasadny, Patricia A Seymour, Christopher Schmidt, Mihaly Hajós, Raymond S Hurst, Jayvardhan Pandit, and Christopher J. O'Donnell

J. Med. Chem., **Just Accepted Manuscript** • DOI: 10.1021/acs.jmedchem.5b00300 • Publication Date (Web): 23 Apr 2015

Just Accepted

Journal of Medicinal Chemistry is published by the American Chemical Society. 1155 Sixteenth Street N.W., Washington, DC 20036

The Discovery and Characterization of the α-Amino-3-hydroxy-5-methyl-4-isoxazolepropionic acid (AMPA) Receptor Potentiator *N*-{(3*S*,4*S*)-4-[4-(5-cyano-2-thienyl)phenoxy]tetrahydrofuran-3-yl}propane-2-sulfonamide (PF-04958242)

Christopher L. Shaffer*[,†,‡], Nandini C. Patel[§], Jacob Schwarz[§], Renato J. Scialis[†], Yunjing Wei[§], Xinjun J. Hou[§], Longfei Xie[§], Kapil Karki[§], Dianne K. Bryce[‡], Sarah M. Osgood[†], William E. Hoffmann[‡], John T. Lazzaro[†], Cheng Chang[†], Dina F. McGinnis[‡], Susan M. Lotarski[‡], JianHua Liu[†], R. Scott Obach[†], Mark L. Weber[‡], Laigao Chen[‖], Kenneth R. Zasadny[‖], Patricia A. Seymour[‡], Christopher J. Schmidt[‡], Mihály Hajós[‡], Raymond S. Hurst[‡], Jayvardhan Pandit[§], and Christopher J. O'Donnell*[,§]

[†]Department of Pharmacokinetics, Dynamics and Metabolism, [‡]Neuroscience Research Unit, [§]Worldwide Medicinal Chemistry and [‖]BioImaging Center, Worldwide Research & Development, Groton Laboratories, Pfizer Inc., Groton, CT 06340, USA

ABSTRACT

A unique tetrahydrofuran ether class of highly potent α-amino-3-hydroxy-5-methyl-4-isoxazolepropionic acid receptor potentiators has been identified using rational and structure-based drug design. An acyclic lead compound, containing an ether-linked isopropylsulfonamide and biphenyl group, was pharmacologically augmented by converting it to a conformationally constrained tetrahydrofuran to improve key interactions with the human GluA2 ligand-binding domain. Subsequent replacement of the distal phenyl motif with 2-cyanothiophene to enhance its potency, selectivity and metabolic stability afforded *N*-{(3*S*,4*S*)-4-[4-(5-cyano-2-thienyl)phenoxy]tetrahydrofuran-3-yl}propane-2-sulfonamide (PF-04958242, **3**), whose preclinical characterization suggests an adequate therapeutic index, aided by low projected human oral pharmacokinetic variability, for clinical studies exploring its ability to attenuate cognitive deficits in patients with schizophrenia.

INTRODUCTION

α-Amino-3-hydroxy-5-methyl-4-isoxazolepropionic acid (AMPA) receptors (AMPAR) mediate fast glutamatergic excitatory neurotransmission in the central nervous system, and alterations in their density and subunit composition are involved in dynamically regulating synaptic function.[1] Specifically, AMPAR opening depolarizes neuronal membranes to relieve the Mg^{2+} block of colocalized *N*-methyl-D-aspartate receptors (NMDAR), which increases NMDAR-mediated Ca^{2+} gating[2] that ultimately generates changes in the synaptic morphology and function[1a, 3] thought to underlie learning and memory.[4] A key mechanism of NMDAR-regulated increases in synaptic activity is AMPAR insertion into the synapse.[5] Thus, enhanced AMPAR activation by a positive allosteric modulator ("potentiator")[6] would be expected to augment NMDAR-induced synaptic potentiation. Accordingly, AMPAR stimulation is an attractive mechanism for treating various neurological and psychiatric diseases[7], particularly certain cognitive impairments in schizophrenia[8] since they are hypothesized to primarily result from dysfunction in NMDAR glutamatergic neurotransmission.[9] This theory is supported by clinical studies[9c, 10] in which healthy volunteers receiving acute subanesthetic doses of nonselective NMDAR antagonists (e.g. ketamine) present with schizophrenia-like symptoms including memory deficits. AMPAR potentiators have demonstrated procognitive properties in numerous animal models of hippocampal/cortical function and working memory[6a, 7a, 11] and in small clinical trials.[12] However, excessive AMPAR excitation, via orthosteric or allosteric molecular interactions, can cause motor coordination disruptions[13], neurotoxicity[14] and/or convulsion.[13, 15] Since the effects of variations in AMPAR subtypes (GluA1–4), splice forms (flip (i) and flop (o)) and binding partners on an AMPAR potentiator's therapeutic index (TI) are unknown, it is essential to understand potentiator exposures causing desired versus harmful

effects to identify a safe molecule for clinical testing. Thus, unbound brain compound concentration ($C_{b,u}$), a high-confidence surrogate of interstitial fluid drug concentrations[16] that determine AMPAR ligand-binding domain (LBD) interactions, was deemed the most appropriate exposure value for defining this mechanism-based TI.

Based on these concepts, we previously reported our strategy for identifying and profiling the two structurally unique AMPAR potentiators *N*-{(3*R*,4*S*)-3-[4-(5-cyano-2-thienyl)phenyl]tetrahydro-2*H*-pyran-4-yl}propane-2-sulfonamide (PF-4778574, **1**)[13a] and *N*-((5*S*)-(3-(3-fluoro-4-(pyrrolidin-1-yl)phenyl)-4,5-dihydroisoxazol-5-yl)methyl)propane-2-sulfonamide (PF-4701475, **2**)[13b] (Figure 1). Other AMPAR potentiators of this sulfonamide class, specifically the biarylpropylsulfonamides (*R*)-3,5-difluoro-*N*-(4-(1-((1-methylethyl)sulfonamide)propan-2-yl)phenyl)benzamide (LY450108)[17] and (*R*)-*N*-(2-(4'-(2-(methylsulfonamido)ethyl)-[1,1'-biphenyl]-4-yl)propyl)propane-2-sulfonamide (LY451395, mibampator)[17-18] and the amino indane sulfonamide *N*-[(2*S*)-5-(6-fluoro-3-pyridinyl)-2,3-dihydro-1*H*-inden-2-yl]-2-propanesulfonamide (GSK729327)[19], have demonstrated excellent safety and tolerability in humans. Compounds **1** and **2**, and those within their respective chemical series, were characterized in select in vitro and single-dose in vivo assays assessing AMPAR-dependent activities related to nootropic effects and safety. Due to the aforementioned complex functional heterogeneity of AMPARs and the lack of a clear understanding of the optimal AMPAR-subtype specificity profile for TI maximization, potentiator binding affinity and functional potency were determined in rodent brain tissue expected to express a native mixture of AMPAR subunits and their associated proteins to afford composite pharmacological values. Functional activity was further evaluated in recombinant cell lines stably expressing human GluA2i and GluA2o, since other AMPAR potentiators bind within these flip/flop

domains[20], and structure-based drug design (SBDD) using X-ray crystal structures of the LBD of human GluA2o[13b] iteratively informed GluA2-based structure-activity relationships (SAR). For memory-related effects (i.e. "efficacy") in animal models of pharmacologically provoked NMDAR hypofunction, both **1**[13a] and **2**[13b] reversed the [5*R*,10*S*]-5-methyl-10,11-dihydro-5*H*-dibenzo[a,d]cyclohepten-5,10-imine (MK-801)-generated subiculum-medial prefrontal cortex (PFC) dysfunction in rats, and **1** attenuated ketamine-mediated spatial working memory impairment in nonhuman primates (NHP).[11a] Safety studies with **1** looked for cerebellum-based AMPAR activation (mouse) and motor coordination disruptions (mouse, dog and NHP), as well as convulsions (mouse, rat and dog). The resulting $C_{b,u}$-normalized exposure-response continuum for **1** showed adequate separation between $C_{b,u}$ linked to efficacy and adverse events (AE). Critically, this work with **1** demonstrated an excellent correlation across species of $C_{b,u}$ required for procognitive characteristics and specific AE suggesting a common and translatable exposure-response relationship in rodents and higher-order species. Progressively higher $C_{b,u}$ led sequentially from efficacy to cerebellar 3',5'-cyclic guanosine monophosphate (cGMP) elevation to motor coordination disruptions to convulsion. These initial studies also underscored the need for a potentiator with low human pharmacokinetic variability to ensure highly predictable maximal plasma drug concentrations (C_{max}) due to the clinical dose-capping nature of these threshold-mediated AE.[21] Appropriately, this strategy, and the interspecies relationships it established for four chemically distinct AMPAR potentiators[13, 21-22], aided in the identification of the current clinical candidate *N*-{(3*S*,4*S*)-4-[4-(5-cyano-2-thienyl)phenoxy]tetrahydrofuran-3-yl}propane-2-sulfonamide (PF-04958242, **3**) (Figure 1), which is described herein.

RESULTS AND DISCUSSION

Discovery of the Novel Tetrahydrofuran Ether Series of AMPAR Potentiators. As described previously[13], an internally developed fluorometric imaging plate reader (FLIPR)-based functional assay utilizing mouse embryonic stem (mES) cell-derived neuronal precursors[23] enabled a high throughput screen (HTS) of our corporate compound file that identified two lead chemotypes.[13b, 23] Subsequent SBDD using X-ray crystal structures of the human GluA2o LBD led to the discovery of *N*-((*S*)-1-(3,5-[^{3}H]-2-fluoro-4-((*S*)-5-((1-methylethylsulfonamido)methyl)-4,5-dihydroisoxazol-3-yl)phenyl)pyrrolidin-3-yl)acetamide ([^{3}H]PF-04725379, **4**), a proprietary radioligand, and other active compounds in its dihydroisoxazole series including prototype **2**, which was used to evaluate AMPAR-mediated pharmacology in vivo.[13b] Simultaneously during the HTS, we explored and expanded upon the SAR of the published biarylpropylsulfonamide AMPAR potentiator (*R*)-*N*-[2-(4'-cyano[1,1'-biphenyl]-4-yl)propyl]propane-2-sulfonamide (LY451646, **5**).[24] In this report we describe our medicinal chemistry strategy to ascertain a unique series of AMPAR potentiators with improved efficacy, selectivity, and metabolic stability compared to **5**. This approach was guided by the X-ray structure of **5** bound to the GluA2o LBD and applied known conformational preferences to generate a new lead series of AMPAR potentiators. Additionally, we describe considerations of the physicochemical properties to impart desired absorption, distribution, metabolism and excretion (ADME) characteristics into newly generated molecules. As a result, we identified the novel potentiator **3**, whose complete primary pharmacology and interspecies ADME profiles are revealed.

Prior to achieving an X-ray crystal structure of **5** bound to the human GluA2o LBD, a number of design hypotheses (Figure 2) were explored: investigation of different vectors around the central aromatic ring (e.g. *meta*-substitution and heteroaryl replacement); linker modulation

(e.g. chain length alteration and heteroatom incorporation); sulfonamide variations/replacements; and, a variety of ring-building strategies to restrict the conformational flexibility of the ethylene chain. Synthetic tractability was a key component of the chemistry strategy, often taking advantage of library-enabled routes to rapidly expand our SAR knowledge. In all cases, the physicochemical properties of virtual molecules were carefully considered so that only compounds having desirable properties[25] of oral CNS drugs were prepared. To facilitate the optimization of matter from hit-to-lead through lead development, various libraries were designed and screened (32 μM) in our mES cell-derived functional assay. For the original design hypotheses, neither vector modification (e.g. *meta*-substitution) nor heteroaliphatic ring (e.g. piperidine) replacement of the central aromatic ring afforded compounds with EC_{50} <32 μM. Extending the length of the two-carbon linker between the central aromatic ring and sulfonamide was also an ineffective strategy. However, linker modulations, specifically the incorporation of an ether moiety, proved advantageous. As with the all-carbon-linker analogs, *para*-substitution on the central aromatic ring was favored over *meta*-substitution (Table 1; **6** vs. **8** and **7** vs. **9**). Interestingly, while the 2-cyanophenyl-substituted analog **7** was 2-fold less potent than **5** it had ca. 60% greater efficacy suggesting a possible functionally favorable AMPAR interaction for this distal aromatic substituent.

The X-ray co-crystal structure of **5** bound to the human GluA2o LBD (Protein Data Bank ID: 4LZ5) revealed informative potentiator-AMPAR contacts.[13b] The sulfonamide hydrogen of **5** forms a backbone hydrogen bond to the carbonyl oxygen of Pro-494, while its biaryl group projects across the dimeric LBD filling the symmetrical binding interface. The model structure of **7**, the most functionally efficacious carbon linker ether analog, was docked[26] onto the crystal structure of **5**. This overlay suggested that the 2-cyano group on the distal aromatic ring of **7**

accessed the symmetrical space to the sulfonamide pocket on the other side of the binding motif (Figure 3). The binding model of **7** shows that the 2-cyano group on the distal aromatic ring is precisely positioned to access the symmetrical binding pocket that is occupied by the sulfonamide group and that the ether group is merely serving as a linker between these two pockets. The acyclic amido-alkoxyethane substructure in **7** prompted us to consider the use of physical organic principles of conformational preference to pre-organize the ligand for binding site complementarity to optimize pharmacological activity.[27] Particularly, 1,2-dialkoxy- or 1,2-dihaloethanes, similar in nature to **7**, are known to prefer a conformation favoring the gauche orientation (Figure 4A).[28] The gauche orientation of a 1,2-dialkoxyethane is favored by ca. 0.5 kcal/mol, and, in this case, it affords an opportunity for an intramolecular hydrogen bond within **7** between its sulfonamide hydrogen and ether oxygen. Therefore, it was hypothesized that further constraint, via a carbo- or heterocycle, should enhance the conformational preference imparted to the acyclic series by the gauche effect. Using 5- or 6-membered rings anchored on the ethylene linker within **7** (Figure 4A), a number of conformationally restricted analogs were designed to afford both *trans*- and *cis*-isomers (Figure 4B). Additional analyses of these virtual compounds by superimposing their structures onto the crystal structure of **5** indicated the *cis*-isomers were optimal to match the bioactive conformations. Consistent with prior findings[29], further consideration of the physicochemical properties of these molecules allowed additional refinement and selection of the *cis*-tetrahydrofuran (THF) ether analogs as the primary series (Figure 4B, A = O).

A five-step synthetic sequence assembled the *cis*-THF ethers (Scheme 1). Highlights of the synthetic strategy include employing classical resolution to avoid chiral chromatography and late-stage introduction of both the sulfonamide and aromatic substituents to facilitate their

efficient diversification for rapid SAR development. Opening of epoxide **10** by *p*-bromophenol **11** in the presence of a base, such as cesium carbonate, in refluxing dioxane installed the aryl ether group. The resulting alcohol was treated with methanesulfonyl chloride and triethylamine to give diastereomeric **12** (quantitative yield over the two steps). Treatment of **12** with sodium azide afforded the corresponding azide, which was converted to amine **13** via the Staudinger reduction. Classical resolution of **13** with camphorsulfonic acid provided enantiopure **14** (30–35% yield, >99% ee). Alternatively, treatment of mesylate **12** with ammonium hydroxide in isopropanol at 110 °C cleanly afforded racemic *cis*-amine **14** in ca. 80% yield. Next, **14** was reacted with isopropylsulfonylchloride in the presence of 1,8-diazabicyclo[5.4.0]undec-7-ene (DBU) to quantitatively afford sulfonamide **15**, which underwent Suzuki coupling with either boronic acid or ester **16** to effectively generate the desired THF-ethers **17**–**28**. In instances where standard Suzuki coupling conditions were unsuccessful, specifically with 5-membered heteroaryls, either reverse Suzuki coupling or CH-activation enabled the desired product.

[a]Reagents and conditions: a) Cs_2CO_3, $BnNEt_3Cl$, dioxane, reflux, 18 h, quant.; b) MsCl, Et_3N, DCM, 0 °C to rt, 18 h, quant.; c) NaN_3, DMF, 110 °C, 66 h, 85%; d) PPh_3, THF, 0 °C to rt, 18 h, 78%; e) (+)-CSA, IPA/H_2O, 18 h, 30–35%; f) *i*$PrSO_2Cl$, DBU, DCM, 0 °C to rt, 20 h, quant.; g) Boronic acid or boronate ester (**16**), XPhos, $Pd(OAc)_2$, KF, 1:1 MeOH/toluene , 40–75%.

The impact of this ring-incorporation design strategy was immediately reflected in differing functional activity improvements between THF-ether vs. ethyl-ether analogs with constant distal aromatics, such as unsubstituted phenyl (**17** vs. **6**, E_{max} of 125% vs. 32%) or *o*-cyanophenyl (**18** vs. **7**, EC_{50} of 21.9 nM vs. 7350 nM) analogs (Tables 1 and 2). Enantiopurification of **18**

revealed its functional potency was predominately due to its (*3S,4S*)-(**19**) and not its (*3R,4R*)-enantiomer (**20**). For all THF-ether analogs for which both isomers were prepared, the (*3S,4S*)-enantiomer was always most active (data not shown). A model of **19** bound to the human GluA2o LBD showed that it overlays similarly to **7** (Figure 3) in that the *o*-cyano is optimally positioned to access a pocket within the binding site that seems to enhance potency. Compound **19** also had physicochemical properties that translated to high membrane permeability ($P_{app,A\rightarrow B}$ = 32.3 × 10^{-6} cm/s) and no P-glycoprotein-mediated efflux (MDR1 ER = 1.39) suggesting favorable central penetration in vivo. However, its human liver microsomes-derived intrinsic clearance (HLM CL_{int}) was unacceptably high (138 mL/min/kg) since a molecule with low human pharmacokinetic variability was desired due to the known clinical dose-capping nature of AMPAR potentiator-mediated AE.[21] To improve metabolic stability, we reasoned that the facile metabolism of **19** was due to hydroxylation of the *o*-cyanophenyl. Accordingly, functionally equipotent analogs, such as 2-cyano-6-fluoro (**21**) and 2-cyano-4-fluoro (**22**), indeed had lower HLM CL_{int} than **19** (Table 2). However, subsequent modifications that successfully reduced aromatic ring lipophilicity to achieve even lower HLM CL_{int} (e.g. **23**) concomitantly reduced functional potency while increasing the number of hydrogen bond donors, TPSA and P-glycoprotein liability.[30] Alternatively, replacing the distal phenyl group with aromatic heterocycles afforded low HLM CL_{int}, high permeability and no P-glycoprotein susceptibility while retaining acceptable functional potency. Such substitution of the distal phenyl group with more polar heteroaromatics (e.g. pyridine (e.g. **24** and **25**) or pyrimidine (e.g. **26**)) also imparted lower clogP, which tends to decrease the likelihood of *in vivo* toxicity by small molecules.[31] Several 5- or 6-membered aromatic heterocycles were prepared, such as cyanothiophene **3**, cyanothiazole **27** and dimethylpyrazole **28** (Table 2). Compounds **3** and **27** provide a different

vector for the cyano group, which potentially occupies a different binding pocket that could impact flip/flop selectivity. It has been speculated[32] that the smaller serine-754-containing side chain within the flip splice variant creates a pocket having a more favorable binding interaction with the requisite cyano moiety that fills it, resulting in a flip-favoring selectivity for such potentiators. An X-ray co-crystal structure of **3** bound to the human GluA2o LBD (Figure 5) revealed the common hydrogen bond between the sulfonamide and Pro-494, and also showed that the cyano group occupied the same space in the vicinity of Asn-754 as the cyano group in **5**. Of these exemplified compounds, **3**, whose absolute stereochemistry was unambiguously elucidated as the (*3S,4S*)-enantiomer via single crystal X-ray analysis (see Supporting Information), was selected for further profiling since it provided the best overall balance of functional potency and efficacy with desired in vitro ADME properties.

Characterization and Preclinical Profile of 3. Potentiator **3** was carefully profiled in a series of single-dose rodent assays to determine its neuropharmacokinetics and mechanism-mediated exposure-response continuum using the previously described interspecies knowledge for select AMPAR potentiators.[13a, 21-22] Observed animal effects were most likely solely AMPAR-dependent since **3** (10 μM) only inhibited three receptors/transporters and one enzyme within a broad human-based receptor/enzyme selectivity panel (Cerep, 118 targets), with the serotonin transporter (K_i of 530 nM) having the most potent interaction. For each animal dose, $C_{b,u}$ was calculated to define a $C_{b,u}$-normalized AMPAR-dependent exposure-response continuum for **3** to understand separations between $C_{b,u}$ enhancing cognition and disturbing motor coordination, as well as in vitro-in vivo pharmacological correlations. Additionally, animal and human ADME data were generated and used to project human pharmacokinetic

parameters, an efficacious dose and the expected C_{max} variability at this dose. Collectively, these datasets afforded an acute TI that supported the progression of **3** into chronic toxicology studies.

In Vitro Pharmacology. The in vitro pharmacological characterization of **3** used a primary strategy of quantifying its properties in rodent tissues expected to express native populations of AMPARs and their associated proteins; a good correlation was found for AMPAR potentiator functional potencies in mouse and human ES cell-derived neurons suggesting interspecies consistency.[23] Using the proprietary radioligand [^{3}H]**4**[13b], **3** had a mean K_i of 170 nM in a rat cortical homogenate. Functionally, **3** showed a glutamate-dependent AMPAR positive allosteric modulation of *S*-AMPA-evoked current in rat primary cortical neurons (EC_{50} of 43±10 nM, ca. 5-fold increase of the maximal *S*-AMPA-induced current; Supporting Information) and *S*-AMPA-mediated Ca^{2+} influx measured in mouse ES cell-derived neuronal precursors (EC_{50} of 310 nM, E_{max} of 110%) and recombinant human GluA2i (EC_{50} of 24 nM, E_{max} of 124%) and GluA2o (EC_{50} of 880 nM, E_{max} of 108%) (Table 3).

Neuropharmacokinetics. Single- (CD-1 mouse) or multiple- (rat) time point neuropharmacokinetics studies were performed with **3** in rodents (Supporting Information) prior to respective in vivo pharmacology tests to optimize both dose selection and the time of pharmacodynamic assessment(s). Furthermore, doses within the respective species-specific pharmacology models (except the mouse rotarod assay) were assumed to have the same dose-$C_{b,u}$ relationship as in the neuropharmacokinetics studies and, thus, their $C_{b,u}$ were extrapolated linearly from the neuropharmacokinetics data to define the exposure-response relationships of **3** at a specific time point post-dose. Thirty minutes after a single dose (1.78 mg/kg, SC) of **3**, CD-1 mice had a mean ± SD total plasma compound concentration (C_p) of 242±106 ng/mL and total brain compound concentration (C_b) of 247±26 ng/mL (equating to a $C_{b,u}$ of 12.0±1.3 nM using

the rat unbound fraction of compound in brain homogenate ($f_{u,b}$) of 0.019), which afforded a C_b:C_p of 1.1±0.3. After a single dose (1 mg/kg, SC) to Sprague-Dawley rats, **3** demonstrated a similar terminal half-life ($t_{1/2}$) in plasma (0.76 h), cerebrospinal fluid (0.71 h) and brain (0.53 h), and a T_{max} of 0.75 h within each neuromatrix. Consistent with the in vitro data predicting it to be a highly permeable non-P-glycoprotein substrate (Table 2), **3** afforded $AUC_{0–Tlast}$-derived ratios suggesting it is readily brain penetrant (C_b:C_p of 1.5) with net equilibrium at the blood-brain barrier ($C_{b,u}$:$C_{p,u}$ of 0.59) (Table 4). Similarly, an IV bolus (0.01 mg/kg) neuropharmacokinetics study, performed in urethane-anesthetized rats under paired-pulse facilitation (PPF) assay conditions, showed **3** had parallel $t_{1/2}$ in each neurocompartment, a C_b:C_p of 2.6 and $C_{b,u}$:$C_{p,u}$ of 1.0. The data suggest urethane anesthesia has no significant effect on the neuropharmacokinetics of **3** in rats.

In Vivo Pharmacology. Compound **3** was evaluated in specific rodent pharmacology models to define the relationship between its $C_{b,u}$ and AMPAR-mediated effects. Collectively, this allowed a $C_{b,u}$-normalized exposure-response continuum for **3** across multiple models of AMPAR-dependent mechanism, safety and procognitive properties ("efficacy") to determine its single-dose TI (Table 3). From a mechanism perspective, **3** was first assessed for its ability to elevate cerebellar cGMP in CD-1 mice, where it showed statistically significant increases (P <0.05 vs. vehicle-treated animals) 0.5 h after receiving a dose of 1.0 mg/kg, SC (Figure 6A). Based on the satellite CD-1 mouse neuropharmacokinetics study (1.78 mg/kg, SC) and assuming stationary pharmacokinetics at all tested doses, the projected mean $C_{b,u}$ at this cGMP-increasing dose was 6.7 nM. Subsequently, the ability of **3** to produce motor deficits was assessed in C57BL/6J mice undergoing an accelerating rotarod test since prior data with **1** defined a very close relationship between $C_{b,u}$ decreasing fall latency in this mouse assay to those causing

movement-related tremors/ataxia in NHP.[13a] Potentiator **3** caused statistically significant (P <0.05) motor deficits in mice 0.5 h after 0.32 mg/kg, SC (Figure 6B), which corresponded to a mean $C_{b,u}$ of 10.8 nM (Table 3).

For efficacy, **3** was tested in two contemporary rat models of pharmacologically provoked NMDAR hypofunction[33]: MK-801-induced subiculum-medial PFC dysfunction[11b] and ketamine-disrupted spatial working memory in the radial arm maze (RAM).[34] In the electrophysiological model, an initial cumulative IV dose-response study (0.001 to 0.01 mg/kg, N=5) was conducted with **3**, and a significant (P <0.01) reversal of the disruptive effects of MK-801 on both cortical electroencephalography (EEG) and PPF were observed following 0.01 mg/kg, IV (Figure 7A). For each dose, $C_{b,u}$ was projected linearly from the $C_{b,u}$ (0.77 nM) observed at 5 min post-dose in the 0.01 mg/kg, IV neuropharmacokinetics study performed under identical assay conditions. A Spearman-Karber analysis revealed an effective dose for 50% of animals (ED_{50}) of 0.003 mg/kg ($C_{b,u}$ of 0.23 nM). Subsequently, a single (i.e. non-cumulative) 0.01 mg/kg, IV time course study was conducted for pharmacokinetic/pharmacodynamic (PK/PD) modeling (Figure 7B); mean onset of the reversal by **3** of the MK-801-dependent PPF disruption was 8±3 min post-dose ($C_{b,u}$ of ca. 0.77 nM). Using a link model, the estimated slope of **3** to reverse the MK-801-induced PPF disruption was 14.2 %•mL/ng, the population mean baseline (i.e. MK-801-mediated disruption) was 79.2% and the K_{e0} was estimated to be 1.93 h^{-1}. Before the MK-801 disruption, the percent of low frequency delta power for untreated rats was 38%. The PD response observed in the PPF experiment ranged from 0% to 73% of the reversal of the MK-801-induced disruption, hence the model may reliably predict the extent of this reversibility up to an inhibitory concentration maximum of 73%. The modeling results indicate that in rats **3** is able to reverse 50% of the MK-801-induced PPF disruption at a C_p of 1.5 ng/mL, which, based on the

IV bolus neuropharmacokinetics data, equates to a $C_{b,u}$ of 0.18 nM (Table 3). As reported[11b] for another AMPAR potentiator in this electrophysiological model, the restorative effects of **3** were fully blocked by pretreatment (1 mg/kg, IV; 10 min after MK-801 administration and 20 min before dosing **3**) with the selective AMPAR antagonist (*S*)-3-(2-chlorophenyl)-2-[2-(6-diethylaminomethyl-pyridin-2-yl)-vinyl]-6-fluoro-3*H*-quinazolin-4-one (CP-465022)[35] (data not shown).

Results in this electrophysiological assay provided the theoretical basis for studying the ability of **3** to curb the disruptive effects of the NMDAR antagonist ketamine on spatial working memory in rats since monosynaptic projection from the hippocampus/subiculum to the medial PFC contributes to working memory[36] and such dysfunction is implicated in the decreased cognitive performance of patients with schizophrenia.[37] Thus, employing a spatial working memory version of the RAM[34], **3** significantly attenuated the ketamine-evoked working memory errors at doses of 0.0032 to 0.032 mg/kg, SC (Figure 8), which equated to projected $C_{b,u}$ of 0.029 to 0.29 nM (Table 3) per the subcutaneous rat neuropharmacokinetics study. As compared to the ketamine-treated group, the 0.032 mg/kg dose also significantly improved several other performance indices (data not shown): it decreased the average time to maze completion; it increased the average number of choices prior to first error; and, it increased the percentage of correct choices on the maze. The data suggest increased glutamatergic neurotransmission produced by **3** afforded significant protection from the ketamine-dependent deficits in spatial working memory in a hormetic exposure-response fashion typical of procognitive agents.[11a, 38]

Once demonstrating both electrophysiological and behavioral effects in rats, **3** was further studied in rats using 2-deoxy-2-[^{18}F]fluoro-D-glucose (FDG) positron emission tomography (PET) as a potential methodology for determining a clinically translatable central biomarker of

AMPAR potentiation. Prior FDG-PET studies with **5** in rats[39] and NHP[40] revealed increased cerebral glucose metabolism rotating from cortical regions to the cerebellum at $C_{b,u}$ paralleling the behavioral transition from procognitive effects (rat and NHP) to elevation in cerebellar cGMP (rat) and motor coordination disruptions (NHP). Thus, FDG-PET studies strategically used doses of **3** (0.027, 0.08 and 0.60 mg/kg, SC) affording at the time of FDG administration maximal $C_{b,u}$ of 0.3 to 6.7 nM, which showed activity in the rat RAM and mouse cerebellar cGMP models, respectively (Table 3). In rats, **3** produced significant increases in FDG uptake (P <0.05 vs. vehicle-treated animals) in cortex and cerebellum (Figure 9A). As observed with **5**, the magnitude of increased FDG uptake, as measured by the number of significantly increased voxels within a brain region of interest, caused by **3** had an opposite pattern in cortex and cerebellum. Specifically, the **3**-dependent FDG-uptake increase at the low dose, which afforded a $C_{b,u}$ of 0.3 nM that showed the most robust effects in the rat RAM, was almost exclusively within the cortex vs. the cerebellum (210 vs. 6 significantly increased voxels). Conversely, FDG-uptake at the high dose, which yielded the minimally effective cGMP-elevating $C_{b,u}$ of 6.7 nM, was almost exclusively within the cerebellum vs. the cortex (1182 vs. 58 significantly increased voxels) (Figure 9B). Since small molecule concentrations are essentially homogeneous across brain regions[16b], these data suggest that different concentrations of **3** are required to selectively (and optimally) activate the respective brain regions associated with procognitive effects (e.g. cortex) and motor coordination (e.g. cerebellum), which may be due to intrinsically different biophysical properties of circuit-specific AMPAR subpopulations. As in the rat PPF model, these increases in FDG uptake were completely blocked by pretreatment (3.2 mg/kg, SC; 30 min before dosing **3**) with the AMPAR antagonist CP-465022 (data not shown). Subsequently, a similar FDG-PET-based exposure-response relationship was determined for **3** in

NHP[41] suggesting this methodology could be considered as a potential translatable central biomarker for both efficacy- and safety-related effects of AMPAR potentiation by **3** in humans.

Interestingly, the $C_{b,u}$ of **3** generating physiological effects in all in vivo assays were just fractions of its concentrations required to produce half-maximal responses in the receptor-based in vitro assays (Table 3). Using the rat K_i and respective $C_{b,u}$, in vivo measures of efficacy and motor deficits occur at projected AMPAR occupancies of <1% and 6%, respectively, and 10 nM was the lowest tested concentration of **3** that clearly enhanced *S*-AMPA-evoked currents in rat cortical neurons (Supporting Information). It is hypothesized[13a] that this phenomenon is due to animals, unlike the employed in vitro systems, having completely intact synergistic neural networks in which only minimal AMPAR potentiation produces enough excitatory neurotransmission for the nonlinear activation of downstream pathways.

Pharmacokinetics and Metabolism. Consistently across all species tested and a 10-fold concentration range, **3** showed a moderate unbound fraction in liver microsomes ($f_{u,LM}$; 0.42 to 0.52), near-unity blood-to-plasma concentration ratio (B/P; 0.82 to 0.90) and low unbound fraction in plasma ($f_{u,p}$; 0.047 to 0.110) (Tables 4 and 5). Single-dose pharmacokinetic studies (Table 4) indicate **3** is rapidly absorbed in rats and dogs (T_{max} ≤0.8 h) following oral (PO) administration. In rats, **3** had very high systemic plasma clearance (*CL*, 169 mL/min/kg, <1% renal), moderate steady-state volume of distribution (V_{ss}, 3.5 L/kg) and moderate oral bioavailability (*F*, 58%). In dogs, its apparent *CL* (11.2 mL/min/kg) and apparent V_{ss} (6.0 L/kg) were moderate. Mean $t_{1/2}$ of **3** were short in rats (≤0.8 h) and moderate-to-long in dogs (6.2 h) and NHP (12.3 h).

Compound **3** demonstrated low and moderate scaled clearance in HLM (CL_H ≤3.8 mL/min/kg) and hepatocytes (CL_H ≤7.1 mL/min/kg), respectively (Table 5). Equivalent studies

in rat (CL_H ≤63.6 mL/min/kg) and dog (CL_H ≤7.4 mL/min/kg) hepatic microsomes were consistent with their respective in vivo *CL* (Table 4). Preliminary in vitro interspecies (rat, dog and human) biotransformation studies with non-radiolabeled **3** (10 μM) found it underwent similar metabolism in dog and human systems where tetrahydrofuran hydroxylation predominates; *O*-dealkylation occurred in all species (Supporting Information). Initial metabolite profiling of plasma (rat and dog) and brain (rat) samples identified both **3** and its *O*-dealkylated metabolite in rat plasma, but only **3** in both dog plasma and rat brain. These studies coupled with those employing major recombinant human cytochrome P450 (rhCYP) isoforms suggest the predominant human clearance pathway for **3** is hepatic CYP-mediated metabolism via CYP2C19 and CYP3A4, both at minimal rates (Table 5). Although a CYP3A4 substrate, no turnover (i.e. $t_{1/2}$ >93 min) of **3** (1 μM) was detected in human intestinal microsomes, consistent with its very low rhCYP3A4 $CL_{int,app}$ (Table 5). The ability of **3** to inhibit seven major CYPs was investigated using HLM and probe substrates, and its lowest IC_{50} was 18 μM (CYP2D6).

For clinical pharmacokinetic parameter projections, both more traditional and newer *in silico* methods were employed. Primarily for the latter methodology, Simcyp software[42] used select experimentally determined data and predicted human pharmacokinetic values to simulate C_p-time profiles for a forecasted efficacious dose of **3** to estimate the clinical variability in C_{max} relative to both C_{eff} and motor coordination disruptions, an exposure threshold-dictated AE. Particularly, this clarified the adequacy of exposure separation between the 95th percentile C_{max}, which corresponds to the lowest C_{max} for the five virtual subjects exhibiting the least extensive metabolism of **3**, and the C_p for movement-related deficits (C_{AE}) at the putative efficacious oral dose. For this exercise, projected clinical C_{eff} (2.4 ng/mL) and C_{AE} (89 ng/mL) were derived using Eq. 2 (Experimental Section) from rodent $C_{b,u}$ corresponding to the highest effective

exposure in the rat efficacy models ($C_{b,u}$ of 0.29 nM) and to the mean value inducing statistically meaningful motor deficits in the mouse rotarod assay ($C_{b,u}$ of 10.8 nM), respectively (Table 3). Using previously described methodology[21], integration of the interspecies in vitro and in vivo metabolism datasets predicts **3** to have in humans a low-to-moderate *CL* (3.12 mL/min/kg) and V_{ss} (0.63 L/kg), resulting in a short-to-moderate $t_{1/2}$ (2.3 h) and a moderate-to-high *F* (81%) (Table 5). The human efficacious dose (0.3 mg) was calculated from these pharmacokinetic parameters, a dosing interval (τ) of 12 h (BID), an assumed 70 kg subject and the desire to maintain C_{eff} as the average C_p at steady-state ($C_{ss,av}$). Using these same C_{eff} and pharmacokinetic parameters, but substituting respective rhCYP-generated $CL_{int,app}$, Simcyp simulations support this projected dosing regimen after a single or multiple (BID for 7 d) dose(s) of 0.3 mg, with low intersubject pharmacokinetic variability and ≤2-fold accumulation at steady-state (Figure 10). Importantly, the modeling of this clinically efficacious dosing regimen of **3** expects no violation of its C_{AE} by its 95th percentile C_{max}. Assuming that both rodent efficacy and motor coordination disruptions are directly translatable, the described animal data suggest that **3** has a single-dose-defined TI of 37 in humans for self-limiting intention tremors, a readily clinically monitorable AE. This, coupled with the projected low variability in human C_p-time profiles, supported the progression of **3** to preclinical safety studies.

On the basis of the described holistically favorable dataset, **3** underwent 90-d regulatory toxicology studies in rats and dogs in which adequate TIs (both C_{max}- and AUC-based) were achieved to advance it to human testing. To date, **3** has been evaluated in eleven clinical trials (see www.clinicaltrials.gov) where it has been safe and well tolerated in healthy volunteers (18–55 y old), in patients (55–70 y old) with age-related sensorineural hearing loss[43] and as adjunctive treatment in subjects with schizophrenia on stable doses of antipsychotics and other

psychotropic medications. Current clinical studies are evaluating **3** for procognitive effects in select neurodisease populations, but principally for its ability to overcome cognitive impairments associated with schizophrenia.

CONCLUSIONS

Rational drug design optimizing both ADME-related physicochemical properties and molecular interactions with the human GluA2 LBD led to the discovery of a new tetrahydrofuran ether class of highly potent AMPAR potentiators. This novel chemical series ultimately afforded *N*-{(3*S*,4*S*)-4-[4-(5-cyano-2-thienyl)phenoxy]tetrahydrofuran-3-yl}propane-2-sulfonamide (PF-04958242, **3**), whose preclinical characterization predicted in humans both a single-dose-defined TI of 37 for self-limiting tremors and low intersubject pharmacokinetic variability. This profile is expected to greatly minimize the potential of eliciting threshold-mediated AEs at a clinically efficacious dosing regimen. Consistent with favorable regulatory toxicology studies that included 90-d studies in rats and dogs, **3** has been safe and well-tolerated in both healthy volunteers (young and elderly) and targeted disease populations, and it is currently being evaluated for its ability to attenuate cognitive deficits in schizophrenia.

EXPERIMENTAL SECTION

General. All compounds were synthesized and fully characterized at Pfizer Worldwide Research & Development (WRD, Groton, CT). Chemicals and solvents of reagent or HPLC grade were supplied by Sigma-Aldrich Corporation, Thermo Fisher Scientific (Waltham, MA) and Mallinckrodt Baker, Inc. (Phillipsburg, NJ). For control matrices, species-specific plasma was acquired from Bioreclamation, Inc. (Hicksville, NY) and rat brain tissue was obtained at WRD. Male CD-1 mice (20 to 25 g) and Sprague-Dawley rats (200 to 275 g) were bought from Harlan Laboratories (Indianapolis, IN) or Charles River Laboratories, Inc. (Wilmington, MA), male C57BL/6J mice (20 to 25 g) were procured from The Jackson Laboratory (Bar Harbor, ME) and beagle dogs (9.4 to 10.3 kg) were sourced from Marshall BioResources (North Rose, New York). Non-naïve NHP (*Macaca fascicularis*, 6.8 to 8.5 kg) resided within the WRD NHP colony (Groton, CT). All animal studies were performed in accordance with the *Guide for the Care and Use of Laboratory Animals*[44] using protocols reviewed and approved by the WRD Institutional Animal Care and Use Committee. Under a protocol approved by Schulman Associates IRB (Cinicnnati, OH), human blood was collected at WRD from three anonymous medication-free male donors on the assay day and a portion of it was used to harvest plasma. Liver microsomes were either prepared and characterized by WRD (Groton, CT) or purchased from BD Gentest (Woburn, MA), cryopreserved human hepatocytes were acquired from Invitrogen (Carlsbad, CA), intestinal microsomes were procured from Xenotech LLC (Lenexa, KS) and recombinant Baculosomes expressing human cytochrome P450 isozymes (CYP1A2, CYP2C8, CYP2C9, CYP2C19, CYP2D6 and CYP3A4) were obtained from PanVera Corporation (Madison, WI). All blood samples were collected into EDTA-containing tubes and processed immediately to obtain plasma, and the collection of neuromatrices from rodents

followed published techniques.[16b] All biomatrices collected for drug quantification were stored at -70 °C until processing for bioanalysis.

Chemistry. ***General Chemistry Procedure.*** All reagents and solvents were used as purchased from commercial sources. Reactions were performed under nitrogen. Mass spectral data were collected on a Micromass ADM atmospheric pressure chemical ionization instrument (LRMS APCI) (Micromass UK Ltd., Manchester, UK). NMR spectra were generated on a Varian 300, 400 or 500 MHz (Varian Medical Systems, Inc., Palo Alto, CA) or Bruker 400 MHz (Bruker Corporation, Coventry, UK) instrument. Chemical shifts were recorded in ppm relative to TMS with multiplicities given as s (singlet), d (doublet), t (triplet), q (quartet), sep (septet), dd (doublet of doublets), dt (double of triplets), ddd (doublet of doublet of doublets), m (multiplet) and br (broad signal). Accurate MS analyses (HRMS) were conducted on an Agilent 6220 TOF mass spectrometer (Agilent Technologies, Wilmington, DE) in electrospray mode in either positive ion mode using an Agilent ZORBAX column (1.8 μ, 3.0 × 50 mm, 60 °C) or negative ion mode using a Waters XBridge column (2.5 μ, 3.0 × 50 mm, 60 °C) (Waters Corporation, Milford, MA). The system was calibrated to greater than 1 ppm accuracy across the mass range prior to analyses according to manufacturer's specifications. The samples were separated using UHPLC on an Agilent 1200 system prior to mass spectrometric analysis. The resulting spectra were automatically lock mass-corrected, and the target mass ions and any confirming adducts (Na^+, NH_4^+) were extracted and combined as a chromatogram. The mass accuracy was calculated for all observed isotopes against the theoretical mass ions derived from the chemical formula using MassHunter software (Agilent Technologies). Low-resolution mass spectra were determined on a Waters/Micromass system. The X-ray diffraction measurements were performed at 298 K on a Bruker SMART APEX CCD Area Detector System equipped with a

graphite monochromator and sealed-tube Cu radiation (1.54178 Å) source. Compound purity was determined by either combustion analysis (Intertek Pharmaceutical Services, Whitehouse, NJ) where the analyses, indicated by the symbols of the elements, were within ±0.4% of the theoretical values or HPLC, confirming it to be ≥95% pure, or by a combination of these two methods. For HPLC (A_{254}), analytes were eluted on a Waters XBridge C18 analytical column (5 µ, 4.6 × 150 mm) at 1.5 mL/min with acetonitrile (solvent A) and water containing 0.1% TFA (solvent B) using the following gradient: 0 to 1.5 min, 5% solvent A in solvent B; 1.5 to 10 min, 5% to 100% A in B; 10 to 11 min, 100% A; 11 to 12.5 min, 100% to 5% A in B. Retention times (t_R) are reported in min and purity is calculated as the percent of total area.

***trans*-4-(4-bromophenoxy)tetrahydrofuran-3-yl methanesulfonate (12).** 3,6-Dioxabicyclo[3.1.0]hexane (**10**, 100 g, 1.16 mol), 4-bromophenol (**11**, 241.1 g, 1.39 mol), cesium carbonate (492 g, 1.51 mol), and benzyltriethylammonium chloride (52.9 g, 0.23 mol) were suspended in dioxane (1 L) and heated at reflux for 18 h. The reaction was cooled to rt, diluted with ethyl acetate and then washed with saturated aqueous sodium carbonate solution. The aqueous layer was extracted with ethyl acetate, the combined organic portions were dried over sodium sulfate and filtered, and the solvent was removed under reduced pressure to provide crude product (354 g, >100%, assumed quantitative), which solidified on standing; this was used without purification in the next step. Material from a smaller-scale experiment carried out in similar fashion was purified by silica gel chromatography for characterization (gradient of 10% to 35% ethyl acetate in heptane) to afford *trans*-4-(4-bromophenoxy)tetrahydrofuran-3-ol as a solid. ^{1}H NMR (400 MHz, $CDCl_3$) δ 7.40 (d, J = 9.1 Hz, 2H), 6.81 (d, J = 9.0 Hz, 2H), 4.67 (m, 1H), 4.41 (br s, 1H), 4.26 (dd, J = 10.4, 4.9 Hz, 1H), 4.05 (dd, J = 10.1, 4.0 Hz, 1H), 3.91 (dd, J = 10.3, 2.1 Hz, 1H), 3.83 (m, 1H), 2.09 (br d, J = 4.5 Hz, 1H).

Triethylamine (181.9 mL, 1.31 mol) was added to a solution of *trans*-4-(4-bromophenoxy)tetrahydrofuran-3-ol (354 g, assumed 300.6 g, 1.16 mol) in methylene chloride (2 L), and the reaction was cooled to 0 °C in an ice bath. Methanesulfonyl chloride (101.3 mL, 1.31 mol) was then added drop-wise, while keeping the reaction temperature <5 °C, and the reaction was stirred at rt for 18 h. Water (1.5 L) was added and the aqueous layer was extracted with methylene chloride. The organics were combined, dried over sodium sulfate and filtered, and the solvent was removed under reduced pressure to yield the brown-oil product (399.6 g, quantitative). Material from a smaller-scale experiment performed similarly was triturated with ethanol for characterization to afford *trans*-4-(4-bromophenoxy)tetrahydrofuran-3-yl methanesulfonate (**12**). ^{1}H NMR (400 MHz, $CDCl_3$) δ 7.42 (d, J = 9.0 Hz, 2H), 6.85 (d, J = 9.1 Hz, 2H), 5.20 (m, 1H), 4.98 (br d, J = 4.6 Hz, 1H), 4.23 (dd, J = 10.5, 4.6 Hz, 1H), 4.16 (dd, J = 11.1, 3.9 Hz, 1H), 4.07 (m, 1H), 4.00 (br dd, J = 10.4, 1.9 Hz, 1H), 3.10 (s, 3H); Elemental analysis calcd for $C_{11}H_{13}BrO_5S$ C: 39.18, H: 3.89, found C: 39.31, H: 3.71; HRMS (ESI$^-$) *m/z* [M + H]$^+$ calcd for $C_{11}H_{13}BrO_5S$ 360.9539, found 360.9543.

***cis*-4-(4-bromophenoxy)tetrahydrofuran-3-amine (13).** Sodium azide (192.6 g, 2.96 mol) was added to a solution of *trans*-4-(4-bromophenoxy)tetrahydrofuran-3-yl methanesulfonate (**12**, 133.2 g, 0.395 mol) in DMF (3 L) and the reaction was heated at 110 ^{o}C for 66 h. The reaction was cooled to rt and water (12 L) was added. This reaction was conducted a total of three times on the same scale and the combined batches were extracted with MTBE. The organic layers were then dried over sodium sulfate and the solvent removed under reduced pressure to afford *cis*-3-azido-4-(4-bromophenoxy)tetrahydrofuran as a red-brown oil contaminated with 18% DMF (corrected yield of 286.7 g, 85%). ^{1}H NMR (400 MHz, $CDCl_3$) δ 7.41 (d, J = 9.0 Hz, 2H),

6.83 (d, *J* = 9.1 Hz, 2H), 4.90 (ddd, *J* = 5.4, 5.4, 4.4 Hz, 1H), 4.17 (dd, *J* = 10.0, 5.6 Hz, 1H), 4.09 (dd, *J* = 8.7, 5.8 Hz, 1H), 4.00 (m, 1H), 3.93–3.97 (m, 2H).

A solution of *cis*-3-azido-4-(4-bromophenoxy)tetrahydrofuran (286.7 g, 1.01 mol) in THF (1.25 L) was cooled to 0 °C and treated with triphenylphosphine (278 g, 1.06 mol). The reaction was allowed to warm to rt and stirred for 18 h, after which water (53 mL) was added and the reaction was further stirred at rt for 66 h. Solvent was removed under reduced pressure and the residue was mixed with diethyl ether. The supernatant was decanted and the solvent was removed under reduced pressure to provide a residue, which was filtered through a short plug of silica gel (gradient of 0% to 5% methanol in methylene chloride) to afford *cis*-4-(4-bromophenoxy)tetrahydrofuran-3-amine (**13**, 155 g) and impure material (366 g). An acid/base extraction of the impure material yielded additional **13** (combined yield of 203.5 g, 78%).

Resolution of *cis*-4-(4-bromophenoxy)tetrahydrofuran-3-amine (13). A mixture of *cis*-4-(4-bromophenoxy)tetrahydrofuran-3-amine (**13**, 191 g, 0.74 mol) and (1*S*)-(+)-10-camphorsulfonic acid (154.2 g, 0.66 mol) was dissolved in 2-propanol (2.4 L) and water (100 mL) at reflux. The clear solution was cooled to rt over 18 h, and the resulting crystals were isolated, washed and dried to afford the (+)-camphorsulfonic acid salt of (3*S*,4*S*)-4-(4-bromophenoxy)tetrahydrofuran-3-amine (139.2 g, 0.284 mol) with an 85% ee. Recrystallization from 2-propanol (1.2 L) and water (70 mL) provided the (+)-camphorsulfonic acid salt of (3*S*,4*S*)-4-(4-bromophenoxy)tetrahydrofuran-3-amine (113.2 g, 31% yield). Chiral HPLC, using a Chiralpak IA column (4.6 × 250 mm) at 0.7 mL/min with heptanes:isopropanol:diethylamine (v/v/v, 80:20:0.2), determined 98.7% ee at 220 nm and 99.4% ee at 260 nm with a t_R of 14.7 min. ^{1}H NMR (300 MHz, DMSO-d_6) δ 8.23 (br s, 3H), 7.52 (d, *J* = 9.0 Hz, 2H), 6.99 (d, *J* = 8.8 Hz, 2H), 5.04 (m, 1H), 3.96–4.10 (m, 3H), 3.78–3.84 (m, 2H), 2.85 (d, *J* = 14.7 Hz, 1H), 2.66–2.73

(m, 1H), 2.35 (d, J = 14.7 Hz, 1H), 2.19–2.28 (m, 2H), 1.76–1.94 (m, 2H), 1.29 (d, half of AB q, J = 10 Hz, 1H), 1.23 (d, half of AB q J = 10 Hz, 1H), 1.05 (s, 3H), 0.74 (s, 3H); Elemental analysis calcd for $C_{10}H_{12}BrNO_2 \bullet C_{10}H_{16}O_4S$ C: 48.98, H: 5.75, N: 2.86, found C: 49.15, H: 5.40, N: 2.80; HRMS (ESI$^-$) m/z $[M + H]^+$ calcd for $C_{10}H_{12}BrNO_2$ 258.0124, found 258.0125.

The (3*S*,4*S*)-4-(4-bromophenoxy)tetrahydrofuran-3-amine (+)-camphorsulfonic acid salt (126.8 g, 0.258 mol) was washed with 2 N aqueous sodium hydroxide solution and extracted three times with methylene chloride. The organic layers were combined and the solvent was removed under reduced pressure to provide (3*S*,4*S*)-4-(4-bromophenoxy)tetrahydrofuran-3-amine (**14a**, 65.6 g, 98% yield, 99% ee) as a white solid.

Subsequently, the combined mother liquors, enriched in (3*R*,4*R*)-4-(4-bromophenoxy)tetrahydrofuran-3-amine, were washed with 2 N sodium hydroxide and extracted with methylene chloride. The combined organic layers were dried over sodium sulfate and the solvent was removed under reduced pressure to give a residue (156.3 g, 0.606 mol of product and its enantiomer). This material was combined with (1*R*)-(-)-10-camphorsulfonic acid (126.2 g, 0.54 mol) and dissolved in 2-propanol (1.65 L) and water (100 mL) at reflux. The clear solution cooled to rt over 18 h and the resulting crystals were isolated, washed and dried to generate the (-)-camphorsulfonic acid salt of (3*R*,4*R*)-4-(4-bromophenoxy)tetrahydrofuran-3-amine (152.6 g, 90% ee). The previously described recrystallization afforded the (-)-camphorsulfonic acid salt of (3*R*,4*R*)-4-(4-bromophenoxy)tetrahydrofuran-3-amine as a white solid (132 g, 36% yield). Chiral HPLC, using a Chiralpak IA column (4.6 × 250 mm) at 0.7 mL/min with heptanes:isopropanol:diethylamine (v/v/v, 80:20:0.2), determined 99.0% ee at 220 nm and 99.7% ee at 260 nm with a t_R of 12.6 min.

***cis*-*N*-[4-(4-bromophenoxy)tetrahydrofuran-3-yl]propane-2-sulfonamide (15).** 1,8-Diazabicyclo[5.4.0]undec-7-ene (53 mL, 0.35 mol) was added to a solution of *cis*-4-(4-bromophenoxy)tetrahydrofuran-3-amine (**13**, 65.6 g, 0.254 mol) in methylene chloride (500 mL). The reaction mixture was cooled to 0 °C and propane-2-sulfonyl chloride (31.2 mL, 0.28 mol) was added drop-wise. The mixture was then stirred at rt for 18 h. Over the course of 20 h, the reaction was monitored by ^{1}H NMR and additional propane-2-sulfonyl chloride (2 × 2.8 mL, 25 mmol) was added. Water (500 mL) was added and the layers were separated. The aqueous layer was extracted with methylene chloride, the combined organic layers were dried over sodium sulfate and filtered, and the solvent was removed under reduced pressure. The residue was dissolved in methylene chloride and washed with aqueous 1 N hydrochloric acid (2 × 300 mL), dried over sodium sulfate and filtered, and the solvent was removed under reduced pressure to provide *cis*-*N*-[4-(4-bromophenoxy)tetrahydrofuran-3-yl]propane-2-sulfonamide (**15**, 92.5 g, quantitative) as an orange/brown oil. ^{1}H NMR (500 MHz, $CDCl_3$) δ 7.41 (d, J = 9.0 Hz, 2H), 6.78 (d, J = 9.0 Hz, 2H), 4.81 (d, J = 9.5 Hz, 1H), 4.75 (ddd, J = 5.9, 4.4, 1.8 Hz, 1H), 4.26–4.18 (m, 1H), 4.17–4.11 (m, 2H), 3.93 (dd, J = 10.7, 1.7 Hz, 1H), 3.69 (t, J = 8.7 Hz, 1H), 3.15 (sep, J = 6.8 Hz, 1H), 1.38 (d, J = 6.8 Hz, 3H), 1.35 (d, J = 6.8 Hz, 3H); ^{13}C NMR (125 MHz, $CDCl_3$) δ 155.6, 132.7, 117.5, 114.5, 76.3, 71.9, 70.2, 55.5, 54.5, 16.6; Elemental analysis calcd for $C_{13}H_{18}BrNO_4S$ C: 42.87, H: 4.98, N: 3.85, found C: 43.38, H: 4.55, N: 3.49; HRMS (ESI-) *m/z* $[M + H]^+$ calcd for $C_{13}H_{18}BrNO_4S$ 364.0213, found 364.0206.

***N*-[(3*S*,4*S*)-4-(4-bromophenoxy)tetrahydrofuran-3-yl]propane-2-sulfonamide (15a).** Compound **15a** was analogously prepared as **15**. Chiral HPLC, using a Chiralpak IA column (4.6 × 250 mm) at 0.7 mL/min with heptanes:isopropanol:diethylamine (v/v/v, 80:20:0.2), determined 99.1% ee at 220 nm and 98.7% ee at 260 nm with a t_R of 15.2 min. Elemental

analysis calcd for $C_{13}H_{18}BrNO_4S$ C: 42.87, H: 4.98, N: 3.85, found C: 42.93, H: 4.85, N: 3.85; HRMS (ESI-) *m/z* $[M + H]^+$ calc. for $C_{13}H_{18}BrNO_4S$ 364.0213, found 364.0217.

***N*-{(3*S*,4*S*)-4-[4-(5-cyano-2-thienyl)phenoxy]tetrahydrofuran-3-yl}propane-2-sulfonamide (3).** Sulfonamide **15a** (0.340 mmol) and (5-cyano-2-thienyl)boronic acid (0.521 mmol), dicyclohexyl(2',4',6'-triisopropylbiphenyl-2-yl)phosphine (XPhos, 0.034 mmol), palladium(II) acetate (0.023 mmol) and potassium fluoride (1.71 mmol) were added to a microwave vial, which was capped and purged three times with nitrogen/vacuum. A 1:1 mixture of degassed methanol:toluene (10 mL) was added and the reaction was subjected to microwave irradiation at 130 °C for 30 min. The solvent was removed under reduced pressure and the residue was partitioned between ethyl acetate and saturated aqueous sodium chloride solution. The aqueous layer was extracted with ethyl acetate (2 × 20 mL), and the organic layers were combined, dried over sodium sulfate and filtered. The filtrate was concentrated under reduced pressure to a residue, which was purified by silica gel chromatography to afford **3** (58%) as a solid. LC-MS *m/z* 393.5 (M+1); ^{1}H NMR (500 MHz, $CDCl_3$) δ 7.58 (d, *J* = 3.9 Hz, 1H), 7.55 (d, *J* = 8.8 Hz, 2H), 7.19 (d, *J* = 3.9 Hz, 1H), 6.95 (d, *J* = 8.8 Hz, 2H), 4.86 (ddd, *J* = 5.8, 4.4, 1.7 Hz, 1H), 4.76 (d, *J* = 9.8 Hz, 1H), 4.30–4.22 (m, 1H), 4.20 (dd, *J* = 10.7, 4.2 Hz, 1H), 4.17 (t, *J* = 8.0 Hz, 1H), 3.98 (dd, *J* = 10.7, 1.7 Hz, 1H), 3.72 (t, *J* = 8.8 Hz, 1H), 3.17 (sep, *J* = 6.8 Hz, 1H), 1.40 (d, *J* = 6.8 Hz, 3H), 1.37 (d, *J* = 6.8 Hz, 3H); ^{13}C NMR (125 MHz, $CDCl_3$) δ 157.5, 151.3, 138.4, 128.1, 126.5, 122.7, 116.3, 114.4, 107.7, 76.2, 72.0, 70.2, 55.6, 54.7, 16.7, 16.6; Elemental analysis calcd for $C_{18}H_{20}N_2O_4S_2$ C: 55.08, H: 5.14, N: 7.14, found C: 55.14, H: 4.99, N: 7.05; HRMS (ESI^-) *m/z* $[M + H]^+$ calcd for $C_{18}H_{20}N_2O_4S_2$ 393.0937, found 393.0931; mp 102–104 °C; $[\alpha]^{20}_D$ = -89.1° (*c* = 0.8, $CHCl_3$).

Pharmacology. ***In Vitro.*** Primary pharmacology assays assessed functional activity using mouse ES cell-derived neuronal precursors[23] and HEK293 cells stably expressing the Ca^{2+}-permeable Q form human AMPAR subunits GluA2i and GluA2o[13a], and binding affinity relative to [^{3}H]**4**[13b] in rat cortical tissue homogenate.[13a] For **3**, its electrophysiological properties were characterized in cultures of rat cortical neurons as described.[13a]

In Vivo. Before in vivo pharmacology experiments, the pharmacokinetics (peripheral and/or central) of **3** were characterized in the appropriate species to determine: total plasma (C_p) and/or brain (C_b) compound concentrations at select times after a specific dose; pharmacokinetic parameters (particularly C_{max} and AUC) and their linearity at doses of pharmacological interest, which allowed the correlation of pharmacodynamics to C_p and/or C_b; T_{max}, which determined pretreatment time in certain assays; and, $t_{1/2}$ that dictated wash-out periods between doses in the rat RAM. For each species, the same vehicle and dosing route used in its pharmacokinetics study were employed in its pharmacodynamics experiment.

Potentiator **3** was studied in select in vivo pharmacology models to understand the relationship between its $C_{b,u}$ and a specific AMPAR-mediated effect, which together allowed comparison to its in vitro pharmacology values; this strategy[13a] provided dose-dependent, temporally normalized and assay-dependent $C_{b,u}$ that could be directly compared across all in vivo models. For terminal assays in which brain tissue was collected from an animal undergoing pharmacodynamic assessment, $C_{b,u}$ (nM units) was determined by measured C_b, compound molecular weight (MW, 392.5 g/mol), rat $f_{u,b}$, an assumed brain tissue density of 1 g/mL and Eq. 1:

$$(C_b / MW) \bullet 1000 \bullet f_{u,b} = C_{b,u} \qquad (1)$$

For the application to ultimate human dose projections and pharmacokinetic simulations, the $C_{b,u}$ from any assay was converted to a human total plasma compound concentration (C_p, ng/mL units) using MW, rat $C_{b,u}$:$C_{p,u}$ (0.59), human $f_{u,p}$ (0.079) and Eq. 2:

$$(C_{b,u} / 1000) \bullet (1 / C_{p,u}:C_{b,u}) \bullet (1 / f_{u,p}) \bullet MW = C_p \quad (2)$$

Mouse Cerebellum Cyclic Guanosine Monophosphate (cGMP) Assay. A modified version[13a] of the procedure of Ryder *et al.*[45] was used to determine the dose-response relationship of **3** (0.1, 0.32, 0.56 or 1.0 mg/kg, SC; N=4–6/dose) to elevate cerebellar cGMP concentrations in CD-1 mice. For each dose group, data were reported as group means ± SEM using X-fold changes in tissue cGMP levels relative to the vehicle-treated group. Doses of **3** were compared to the concurrent vehicle control group using One-way Analysis of Variance (ANOVA) followed by Dunnett's t-test (SigmaStat Version 3.5; Systat Software, Inc., Chicago, IL). A value of P <0.05 indicated a statistically significant effect.

Mouse Rotarod Assay. Employing the described procedure[13a], **3** (0.1, 0.178 or 0.32 mg/kg, SC) was evaluated in C57BL/6J mice (N=12/dose) on the accelerating rotarod.[46] For testing, each mouse was subjected to three consecutive trials on the rods with a 10 s inter-trial interval. The mean fall latency for three trials was calculated and data were reported as group means ± SEM. Doses of **3** were compared to the concurrent vehicle control group using One-way ANOVA followed by Dunnett's t-test (SigmaStat Version 3.5; Systat Software, Inc.). A value of P <0.05 indicated a statistically significant effect. Upon completion of the last trial, a subset of animals (N=2–3/dose) underwent blood and brain sample collection for **3** quantification.

Rat MK-801-Disrupted Cortical Oscillation and Paired-Pulse Facilitation (PPF) Assay. This study quantified the effects of **3** on the disruption of cortical EEG and PPF by the NMDAR antagonist MK-801 (0.05 mg/kg, IV; Tocris Bioscience, Bristol, UK) in urethane-anesthetized rats.[47] This is a preclinical model, which evaluates the subiculum-medial PFC pathway, proposed for studying NMDAR hypofunction of schizophrenia. Experimental procedures were those published by Kiss *et al.*[11b] using male Sprague-Dawley rats (250 to 320 g, N=5) under urethane anesthesia (1.5 mg/kg, intraperitoneal). For the IV dose-response effects of **3**, control waveform averages were first computed using 60 consecutive paired-stimuli over a 10 min period. MK-801 was then administered, and, after a 5-min waiting period, paired-pulse averaging was again conducted over the next two consecutive 5-min time bins. The total MK-801 response was then computed by combining these two averages. At the end of the second 5-min data collection time bin (i.e. 15 min after MK-801 injection), cumulative IV administration of **3** (0.001, 0.003 and 0.01 mg/kg) was initiated. Similar to how the data were handled following MK-801 dosing, 5 min were allowed between each successive injection of **3** and the start of the subsequent averaging. If no effect was observed before the end of the second 5-min averaging period then the two 5-min averages were combined as a single value for that dose and the next IV dose was given. If an effect was observed at any point during the first two averages following a given dose, then two additional 5-min averages were combined as the data point for that dose. The reversal of the MK-801 effects by **3** did not occur in a typical cumulative dose-response manner, but rather as an all-or-none effect with variable threshold doses between animals. Since reversal was an all-or-none effect once the threshold dose in a particular animal was reached, no additional cumulative doses of **3** were given. Subsequently, a PPF time-course study was conducted with a single dose of **3** (0.01 mg/kg, IV; N=3). In this experiment,

responses to the paired-pulse stimulations were recorded continuously and averaged over each consecutive 10-min time-bin for 60 min to obtain the overall time course of **3** activity. Mean effects in the doses of **3** (cumulative-dose study) or time-bins (single-dose study) were compared to both the control and MK-801 doses using a two-tailed Student's *t* test (Microsoft Excel, Microsoft Corporation, Redmond, WA). A value of $P < 0.05$ indicated a statistically significant effect. For the cumulative-dose study, a Spearman-Karber analysis calculated an effective dose for 50% of animals (ED_{50}) to provide an idea of a minimally effective dose.

Pharmacokinetic/Pharmacodynamic Modeling of the PPF Assay. From the IV neuropharmacokinetics study, the C_p of **3** was characterized by an empirical two-compartment model; from the time-course PPF study, the MK-801-induced PPF disruption was modeled as a baseline. A link model was used to describe the slight hysteresis between the reversal of the MK-801-induced PPF disruption and C_p. Since the time course study was only conducted at one dose (0.01 mg/kg, IV), a slope model was used to describe the pharmacodynamic interaction within the effect compartment. Final parameter estimates were obtained using nonlinear mixed-effect modeling with interanimal variability in baseline MK-801-induced PPF disruptions. Model characterization and parameter estimation procedures were performed using NONMEM version V (University of California at San Francisco, CA).

Rat Ketamine-disrupted Spatial Working Memory Radial Arm Maze (RAM). This study's goal was to quantify the ability of **3** to antagonize the ketamine-induced spatial working memory impairments in rats, a model of glutamatergic dysregulation hypothesized to underlie the cognitive deficits in schizophrenia.[34] Prior to RAM, **3** (0.01, 0.032, 0.1, 0.32 and 1 mg/kg, SC) was tested in unhabituated and habituated Long-Evans rats to evaluate its effects on basal locomotor activity and in psychomotor stimulant-induced hyperactivity tests to aid with dose

selection in RAM experiments; **3** had no significant effects on locomotor activities under any condition. Briefly, Long-Evans rats were trained in a spatial working memory version of the RAM task until all animals had reached the training criterion. Performance on the maze was then evaluated 0.5 h after the administration of (±)-ketamine (10 mg/kg, SC; Ketaset, Zoetis, Florham Park, NJ) to animals (N=12/dose) that had received either vehicle or **3** (0.0032, 0.01, 0.032, 0.1 or 0.32 mg/kg, SC) 0.5 h before (±)-ketamine. Working memory errors were reported as group means ± SEM. All dose groups were compared to the vehicle-treated ketamine-disrupted group using a generalized linear mixed model assuming an underlying Poisson distribution followed by a Hochberg's test for multiple post hoc comparisons (SAS Software, SAS Institute, Inc., Cary NC). A value of $P \leq 0.05$ indicated a statistically significant effect.

Rat 2-Deoxy-2-[^{18}F]fluoro-D-glucose Positron Emission Tomography (FDG-PET). This study determined in rats the effect on central activity, as measured by changes in regional brain uptake of FDG, by **3** relative to vehicle. Thirty-six male Sprague-Dawley rats (N=12/group) were deprived of food overnight to ensure fasted glucose levels at the time of PET scanning. A single injection (1 mL/kg, SC) of vehicle (2:98 (v/v) DMSO:30% hydroxypropyl-β-cyclodextrin) or **3** (0.027, 0.08 or 0.60 mg/kg) was administered to each animal within its respective dose group. After 0.5 h, rats were briefly anesthetized with isoflurane (5% and 2% (v/v) in oxygen for knock-down and maintenance, respectively) and given an IV bolus of FDG (ca. 1.8 mCi in 0.5 mL saline, followed by a flush of 0.5 mL saline) via the tail vein. Animals were then allowed to recover and kept awake in their home cage during a 0.75 h FDG-uptake phase. Subsequently, each rat was re-anesthetized with isoflurane (1 to 2% in oxygen) and placed on an animal bed with its brain centered in the field of view of a Focus F220 microPET scanner (Siemens Molecular Imaging, Knoxville, TN). Its head was fixed in place by a tooth bar and ear canal

holders for a 15 min static PET scan at 0.75 to 1 h after FDG injection. Animal breathing rate was monitored and maintained around 40 to 60 breaths per min using a small animal physiological monitoring system (SA Instruments Inc., Stony Brook, NY), and rats were sacrificed using CO_2 immediately after scanning. The PET images were reconstructed into standard uptake values (SUV) by applying corrections for detector normalization, decay, attenuation and scatter using a hybrid 3D OSEM/MAP reconstruction algorithm (microPET Manager, Siemens Molecular Imaging) to a 128 × 128 × 95 matrix with a voxel size of 0.6 mm × 0.6 mm × 0.796 mm. Then, the images were coregistered and mapped to a standard rat brain atlas for identification of brain regions using a proprietary registration algorithm employing a rigid-body transform. The PET image of each animal was normalized by its mean whole brain uptake to remove the whole brain FDG uptake variations among animals. Subsequently, Analysis of Functional NeuroImages (AFNI) software[48] was applied to perform voxel-by-voxel statistical parametric mapping via an unpaired t test to look for significant changes in FDG uptake by comparing the two **3**-treated groups to the vehicle-treated group. For the AFNI analysis, the PET image voxel size was resampled to be 0.5 mm × 0.5 mm × 0.5 mm. A correction for multiple comparisons was made within the AFNI analysis package by selecting a voxel cluster size generated from a Monte Carlo simulation. Only voxels passing the t test (P <0.05) and satisfying the cluster size constraints for connectivity were considered significant; only voxels that were significantly increased or decreased between animal groups were identified by the AFNI analysis. For the three groups receiving **3**, the number of voxels with significantly increased FDG uptake compared to the vehicle group within the entire volume of the cortex and cerebellum were counted.

Pharmacokinetics Studies. ***Interspecies Binding Factors.*** Using published procedures[16b, 21], the blood-to-plasma concentration ratio (B/P) and unbound fraction (f_u) in both plasma ($f_{u,p}$) and liver microsomes ($f_{u,LM}$) of **3** (0.05 and 0.5 μM, N=4/species) were determined for Sprague-Dawley rat, beagle dog, cynomolgus monkey and human; its (1 μM, N=4) unbound fraction in Sprague-Dawley rat brain homogenate ($f_{u,b}$) was ascertained similarly. The stability of **3** in each matrix and the optimal incubation/dialysis time were determined separately prior to actual studies.

In Vitro Metabolism. Incubations using interspecies (rat, dog, NHP and human) liver (LM) and intestinal (IM) microsomes and hepatocytes (Hep) and recombinant human cytochrome P450s (rhCYP) were performed as described.[21] Using either the BioBook module in the E-Workbook Suite (IDBS Ltd, Guildford, Surrey, UK) or manual calculation in Microsoft Excel (Microsoft Corp., Redmond, WA), hepatic apparent intrinsic ($CL_{int,app}$) and blood (CL_H) clearances were calculated using the well-stirred model without (LM and Hep) and with (LM) all binding factors.[49]

In Vivo Pharmacokinetics. Individual animal doses were calculated based on respective dose solution concentrations (mg/mL), pretreatment body weights (kg) and dose volume (mL/kg). The actual amount of dose solution administered to each animal was determined by weighing the loaded syringe before and after it was dispensed. All study animals were fasted overnight and for ca. 4 h post-dose.

Mouse. A single dose (1.78 mg/kg) of **3** in 5:5:90 (v/v/v) DMSO:cremophor EL:H_2O (0.178 mg/mL) was administered (10 mL/kg) subcutaneously (SC) to CD-1 (N=3) mice. At 0.5 h post-dose, animals were placed under isoflurane anesthesia for the collection of blood and brain samples.

Rat. Intravenous and Oral Dosing. Jugular vein-cannulated male Sprague-Dawley rats (N=2/dose) received **3** either as a single intravenous bolus (IV, 1 mL/kg, 0.2 mg/kg, 20% hydroxypropyl-β-cyclodextrin) or by oral gavage (PO, 10 mL/kg, 3 mg/kg, 0.5% methylcellulose). For the IV study, blood samples (0.2 mL) were serially collected just before dosing and at 0.083, 0.25, 0.5, 1, 2, 4 and 7 h post-dose; for the PO study, identical sampling occurred at 0.25, 0.5, 1 and 2 h post-dose. *Neuropharmacokinetics.* A single dose (1 mg/kg, SC) of **3** in 2:98 (v/v) DMSO:30% hydroxypropyl-β-cyclodextrin (1 mg/mL) was injected (1 mL/kg) into each male Sprague-Dawley rat. Blood, cerebrospinal fluid (CSF) and brain samples were collected from each animal after isoflurane anesthesia euthanasia at 0.25, 0.5, 1, 2, 4 and 8 h post-dose (N=2/time point). This study was conducted to determine both basic neuropharmacokinetic parameters[16b] and to provide time point-specific $C_{b,u}$ for extrapolating linearly $C_{b,u}$ at a select time point for each dose tested in the rat RAM model. Separately, a single IV-dosed (0.01 mg/kg) rat neuropharmacokinetics study was performed in urethane-anesthetized animals identically paralleling PPF assay conditions. Blood and brain samples were collected from each animal at 5, 10, 15, 30 and 60 min post-dose (N=2/time point) to parallel the full duration of a PPF experiment. The exposure-time data from this study was exclusively used for the PPF model experiments to linearly project $C_{b,u}$ in dose-response studies and to establish from a single-dose study the temporal pharmacokinetic-pharmacodynamic relationship of **3**.

Dog. A single dose (0.1 mg/kg, PO) of **3** in 0.5% methylcellulose was given (1 mL/kg) to each dog (N=3/gender). Blood samples (2 mL) were obtained via the jugular vein just before dosing and at 0.25, 0.5, 1, 2, 6 and 24 h post-dose. For the first 6 h following dosing, animals were continuously monitored by trained lab staff for any readily apparent adverse events.

Nonhuman primate (NHP). A single dose (0.032 mg/kg, SC) of **3** in 1:9 (v/v) cremophor EL:H_2O (1 mL/kg) was administered to the dorsal thoracolumbar area of each NHP (N=2). Blood samples (3 mL) were obtained via a vascular access port just before dosing and at 0.25, 0.5, 1, 2, 4, 6 and 24 h post-dose. After remaining chaired for 2 h post-dose, animals were returned to their home cage. They were again chaired just prior to blood collection at 4, 6 and 24 h post-dose, and released back to their home cage after each blood sampling. Trained lab staff constantly observed each NHP for any readily apparent adverse events for 6 h post-dose.

Quantitative Analysis of 3 in Biological Matrices. The quantification of **3** in interspecies plasma, rat CSF or rodent brain tissue samples was achieved using slightly modified versions of published LC-MS/MS methodologies[16b, 21] with an appropriate internal standard. Mass spectral data were collected using negative ionization in multiple-reaction monitoring scanning mode tracking *m/z* 391.1→284.9 (**3**). Respective matrix lower (LLOQ) and upper limits of quantification were: 0.1 to 100 ng/mL for rodent, dog and human plasma; 0.06 to 6 ng/mL for NHP plasma; 0.1 to 100 ng/mL for rat CSF; and, 0.6 to 60 ng/mL for rodent brain tissue. Analyst 1.4.2 (Applied Biosystems, Foster City, CA) software was used for the acquisition and processing of mass spectral data, as well as analyte quantification performed via weighted ($1/x^2$) linear regression.

Pharmacokinetic Calculations. Pharmacokinetic parameters were calculated by non-compartmental analyses using WinNonlin version 5.2 (Pharsight Corp., Mountain View, CA). The area under the matrix compound concentration-time curve ($AUC_{0-Tlast}$) was calculated using the linear trapezoidal method, the elimination rate constant (k_{el}) was determined by linear regression of the log concentration versus time data during the last observable elimination phase, half-life ($t_{1/2}$) was calculated as $0.693/k_{el}$, and $AUC_{0-\infty}$ was calculated as the sum of $AUC_{0-Tlast}$

and $AUC_{Tlast-\infty}$, which was determined by dividing the plasma concentration at T_{last} by k_{el}. Both maximal total matrix drug concentration (C_{max}) and its time of first occurrence (T_{max}) were taken directly from the matrix compound concentration-time data. Means and standard deviations (SD) were computed when half or greater of the values exceeded the LLOQ; 0 was used if a measured value was <LLOQ. Volume of distribution (V) was calculated by the equation $V = CL$ • (AUMC/AUC), where AUMC is the total area under the first moment-time curve and systemic clearance (CL) was determined by dividing the measured dose by plasma $AUC_{0-Tlast}$. All AUC values were subject weight-normalized.

Biotransformation. To gain a preliminary assessment of the metabolites of **3**, it underwent in vitro biotransformation studies and, subsequently, metabolite profiling of plasma (rat, dog) and brain samples (rat). Briefly, incubations with **3** (10 μM) were performed in interspecies LM (1 mg protein/mL, 30 min incubation) and human hepatocytes (0.75×10^6 viable cells/mL, 2.5 h incubation) using reported[21] experimental and bioanalytical procedures. Plasma and brain samples came from single-dose toxicology studies and were processed similarly to identical samples undergoing **3** quantification only.

Predicted Human Pharmacokinetics and Simcyp Simulations for 3. Using precisely the same published[21] methodology and simulation criteria, clinical pharmacokinetic parameters were projected and a combination of these parameters and rhCYP $CL_{int,app}$ were incorporated into Simcyp v8.10 SP1 (Certara, L.P., St. Louis, MO) to simulate human C_p-time profiles for a forecasted clinically relevant single or multiple oral dose(s) (0.3 mg) of **3**. The virtual population (N=100) was constructed by 10 trials (N=10/trial), 18–65 y old healthy volunteers (34% female), a fixed seed value of 1, fasted, 250 mL fluid intake with dose, no contribution of renal clearance to **3** systemic clearance, and a coefficient of variation of 30%.

ASSOCIATED CONTENT

Supporting Information. Synthetic procedures and characterization data for **3** and **6**–**28**, single X-ray crystallography data for **3**, X-ray data collection and refinement statistics for protein/ligand complexes, summary of electrophysiology experiments with **3** in rat primary cortical neurons, and preclinical pharmacokinetics and biotransformation data for **3**. This material is available free of charge via the Internet at http://pubs.acs.org.

Accession Codes. Coordinates and structure factors have been deposited to the Protein Data Bank for human GluA2o complexes of **5** (LY451646) (ID: 4LZ5) and **3** (PF-04958242) (ID: 4X48).

AUTHOR INFORMATION

Corresponding Authors

*(C.L.S.) Tel +1 617.395.0769. E-mail: Christopher.L.Shaffer@pfizer.com

*(C.J.O.) Tel +1 860.715.4118. E-mail: Christopher.J.ODonnell@pfizer.com

Present Addresses

(C.L.S, N.C.P., X.J.H., S.M.L., M.L.W, C.J.S.) Pfizer Worldwide Research & Development, 610 Main Street, Cambridge, MA 02139

(J.S.) Genentech, Inc., South San Francisco, CA 94080

(K.K.) Gilead Sciences, Inc., Foster City, CA 94404

(D.K.B.) Merck Research Laboratories, Boston, MA 02115

(D.F.M.) Mars Petcare, Franklin, TN 37067

(K.R.Z.) inviCRO, LLC, Boston, MA 02110

(P.A.S.) Mnemosyne Pharmaceuticals, Inc., Providence, RI 02930

(M.H.) Yale School of Medicine, New Haven, CT 06510

(R.S.H.) FORUM Pharmaceuticals, Watertown, MA 02472

Notes

At the time that this work was completed, all authors were full-time employees of Pfizer Inc. and owned and/or held options and/or restricted stock units for the company's publicly traded shares. At the time that this work was disclosed, only some authors were full-time employees of Pfizer Inc. and thus they maintained the aforementioned equity interest(s).

ACKNOWLEDGMENTS

The authors acknowledge: Roberta Dorow, Michael W. Fichtner, John M. Humphrey, Morgan Stewart, Don Wishka and Kevin Witter for chemistry scale-up support; Eric S. Marr and Brian Samas for GluA2o protein purification and protein-ligand complex crystallization; Curt Christoffersen for performing the in-life portion of the NHP pharmacokinetics study; and, Haojing Rong for conducting initial Simcyp simulations.

ABBREVIATIONS USED

AMPA(R), α-amino-3-hydroxy-5-methyl-4-isoxazolepropionic acid (receptors); NMDAR, *N*-methyl-D-aspartate receptors; GluA2o, the flop splice form of the AMPAR subtype 2; TI, therapeutic index; $C_{b,u}$, unbound brain compound concentration; LBD, ligand-binding domain; PFC, prefrontal cortex; AE, adverse event(s); mES, mouse embryonic stem; HLM, human liver microsomes; CL_{int}, intrinsic clearance; PPF, paired-pulse facilitation; FDG, 2-deoxy-2-[^{18}F]fluoro-D-glucose; CYP, cytochrome P450.

REFERENCES

1. (a) Malinow, R.; Malenka, R. C. AMPA receptor trafficking and synaptic plasticity. *Annu. Rev. Neurosci.* **2002,** *25*, 103-126. (b) Huganir, R. L.; Nicoll, R. A. AMPARs and synaptic plasticity: the last 25 years. *Neuron* **2013,** *80*, 704-717.

2. Lynch, G. Memory enhancement: the search for mecahnism-based drugs. *Nat. Neurosci.* **2002,** *5*, 1035-1038.

3. Lynch, G.; Gall, C. M. Ampakines and the threefold path to cognitive enhancement. *Trends Neurosci.* **2006,** *29*, 554-562.

4. Morris, R. G. M. Long-term potentiation and memory. *Philos. Trans. R. Soc. Lond. B Biol. Sci.* **2003,** *358*, 643-647.

5. Sun, X.; Zhao, Y.; Wolf, M. E. Dopamine receptor stimulation modulates AMPA receptor synaptic insertion in prefrontal cortex neurons. *J. Neurosci.* **2005,** *25*, 7342-7351.

6. (a) Black, M. D. Therapeutic Potential of Positive AMPA Modulators and Their Relationship to AMPA Receptor Subunits. A Review of Preclinical Data. *Psychopharmacology* **2005,** *179*, 154-163. (b) Grove, S. J. A.; Jamieson, C.; Maclean, J. K. F.; Morrow, J. A.; Rankovic, Z. Positive allosteric modulators of the α-amino-3-hydroxy-5-methyl-4-isoxazolepropionic acid (AMPA) receptor. *J. Med. Chem.* **2010,** *53*, 7271-7279.

7. (a) O'Neill, M. J.; Bleakman, D.; Zimmerman, D. M.; Nisenbaum, E. S. AMPA Receptor Potentiators for the Treatment of CNS Disorders. *Curr. Drug Targets CNS Neurol. Disord.* **2004,** *3*, 181-194. (b) Zarate Jr., C. A.; Manji, H. K. The role of AMPA receptor modulation in the treatment of neuropsychiatric diseases. *Exp. Neurol.* **2008,** *211*, 7-10.

8. (a) Millan, M. J.; Agid, Y.; Brune, M.; Bullmore, E. T.; Carter, C. S.; Clayton, N. S.; Connor, R.; Davis, S.; Deakin, B.; DeRubeis, R. J.; Dubois, B.; Geyer, M. A.; Goodwin, G. M.;

Gorwood, P.; Jay, T. M.; Joels, M.; Mansuy, I. M.; Meyer-Lindenberg, A.; Murphy, D.; Rolls, E.; Saletu, B.; Spedding, M.; Sweeney, J.; Whittington, M.; Young, L. J. Cognitive dysfunction in psychiatric disorders: characteristics, causes and the quest for improved therapy. *Nat. Rev. Drug Discov.* **2012,** *11*, 141-168. (b) Moghaddam, B.; Javitt, D. C. From revolution to evolution: the glutamate hypothesis of schizophrenia and its implication for treatment. *Neuropsychopharmacology* **2012,** *37*, 4-15. (c) Collingridge, G. L.; Volianskis, A.; Bannister, N.; France, G.; Hanna, L.; Mercier, M.; Tidball, P.; Fang, G.; Irvine, M. W.; Costa, B. M.; Monaghan, D. T.; Bortolotto, Z. A.; Molnar, E.; Lodge, D.; Jane, D. E. The NMDA receptor as a target for cognitive enhancement. *Neuropharmacology* **2013,** *64*, 13-26.

9. (a) Olney, J. W.; Farber, N. B. Glutamate receptor dysfunction and schizophrenia. *Arch. Gen. Psychiatry* **1995,** *52*, 998-1007. (b) Goff, D. C.; Coyle, J. T. The emerging role of glutamate in the pathophysiology and treatment of schizophrenia. *Am. J. Psychiatry* **2001,** *158*, 1367-1377. (c) Javitt, D. C. Glutamate and schizophrenia: phencyclidine, N-methyl-D-aspartate receptors, and dopamine-glutamate interactions. *Int. Rev. Neurobiol.* **2007,** *78*, 69-108.

10. Krystal, J. H.; Karper, L. P.; Seibyl, J. P.; Freeman, G. K.; Delaney, R.; Bremner, J. D.; Heninger, G. R.; Bowers, J., M.B.; Charney, D. S., Subanesthetic effects of the noncompetitive NMDA antagonist, ketamine, in humans. Psychotomimetic, perceptual, cognitive, and neuroendocrine responses. *Arch. Gen. Psychiatry* **1994,** *51*, 199-214.

11. (a) Roberts, B. M.; Holden, D. E.; Shaffer, C. L.; Seymour, P. A.; Menniti, F. S.; Schmidt, C. J.; Williams, G. V.; Castner, S. A., Prevention of ketamine-induced working memory impairments by AMPA potentiators in a nonhuman primate model of cognitive dysfunction. *Behav. Brain Res.* **2010,** *212*, 41-48. (b) Kiss, T.; Hoffmann, W. E.; Hajos, M.,

Delta oscillation and short-term plasticity in the rat medial prefrontal cortex: modelling NMDA hypofunction of schizophrenia. *Int. J. Neuropsychopharmacol.* **2011,** *14*, 29-42.

12. Marenco, S.; Weinberger, D. R. Therapeutic Potential of Positive AMPA Receptor Modulators in the Treatment of Neuropsychiatric Disorders. *CNS Drugs* **2006,** *20*, 173-185.

13. (a) Shaffer, C. L.; Hurst, R. S.; Scialis, R. J.; Osgood, S. M.; Bryce, D. K.; Hoffmann, W. E.; Lazzaro, J. T.; Hanks, A. N.; Lotarski, S.; Weber, M. L.; Liu, J.; Menniti, F. S.; Schmidt, C. J.; Hajós, M. Positive allosteric modulation of AMPA receptors from efficacy to toxicity: the interspecies exposure-response continuum of the novel potentiator PF-4778574. *J. Pharmacol. Exp. Ther.* **2013,** *347*, 212-224. (b) Patel, N. C.; Schwarz, J.; Hou, X. J.; Hoover, D. J.; Xie, L.; Fliri, A. J.; Gallaschun, R. J.; Lazzaro, J. T.; Bryce, D. K.; Hoffman, W. E.; Hanks, A. N.; McGinnis, D.; Marr, E. S.; Gazard, J. L.; Hajos, M.; Scialis, R. J.; Hurst, R. S.; Shaffer, C. L.; Pandit, J.; O'Donnell, C. J. Discovery and characterization of a novel dihydroisoxazole class of α-amino-3-hydroxy-5-methyl-4-isoxazolepropionic acid (AMPA) receptor potentiators. *J. Med. Chem.* **2013,** *56*, 9180-9191.

14. (a) Garthwaite, G.; Garthwaite, J. Mechanisms of AMPA neurotoxicity in rat brain slices. *Eur. J. Neurosci.* **1991,** *3*, 729-736. (b) Brorson, J. R.; Manzolillo, P. A.; Gibbons, S. J.; Miller, R. J. AMPA receptor desensitization predicts the selective vulnerability of cerebellar purkinje cells to excitotoxicity. *J. Neurosci.* **1995,** *15*, 4515-4524.

15. (a) Yamada, K. A. Modulating excitatory synaptic neurotransmission: potential treatment for neurological disease. *Neurobiol. Dis.* **1998,** *5*, 67-80. (b) Qi, J.; Wang, Y.; Jiang, M.; Warren, P.; Chen, G. Cyclothiazide induces robust epileptiform activity in rat hippocampal neurons both in vitro and in vivo. *J. Physiol.* **2006,** *571*, 605-618.

16. (a) Liu, X.; Van Natta, K.; Yeo, H.; Vilenski, O.; Weller, P. E.; Worboys, P. D.; Monshouwer, M. Unbound drug concentration in brain homogenate and cerebral spinal fluid at steady state as a surrogate for unbound concentration in brain interstitial fluid. *Drug Metab. Dispos.* **2009,** *37*, 787-793. (b) Doran, A. C.; Osgood, S. M.; Mancuso, J. Y.; Shaffer, C. L. An evaluation of using rat-derived single-dose neuropharmacokinetic parameters to project accurately large animal unbound brain drug concentrations. *Drug Metab. Dispos.* **2012,** *40*, 2162-2173.

17. Jhee, S. S.; Chappell, A. S.; Zarotsky, V.; Moran, S. V.; Rosenthal, M.; Kim, E.; Chalon, S.; Toublanc, N.; Brandt, J.; Coutant, D. E.; Ereshefsky, L. Multiple-dose plasma pharmacokinetic and safety study of LY450108 and LY451395 (AMPA receptor potentiators) and their concentration in cerebrospinal fluid in healthy human subjects. *J. Clin. Pharmacol.* **2006,** *46*, 424-432.

18. (a) Chappell, A. S.; Gonzales, C.; Williams, J.; Witte, M. M.; Mohs, R. C.; Sperling, R. AMPA potentiator treatment of cognitive deficits in Alzheimer disease. *Neurology* **2007,** *68*, 1008-1012. (b) Trzepacz, P. T.; Cummings, J.; Konechnik, T.; Forrester, T. D.; Chang, C.; Dennehy, E. B.; Willis, B. A.; Shuler, C.; Tabas, L. B.; Lyketsos, C., Mibampator (LY451395) randomized clinical trial for agitation/aggression in Alzheimer's disease. *Int. Psychogeriatr.* **2013,** *25*, 707-719.

19. Ward, S. E.; Harries, M.; Aldegheri, L.; Andreotti, D.; Ballantine, S.; Bax, B. D.; Harris, A. J.; Harker, A. J.; Lund, J.; Melarange, R.; Mingardi, A.; Mookherjee, C.; Mosley, J.; Neve, M.; Oliosi, B.; Profeta, R.; Smith, K. J.; Smith, P. W.; Spada, S.; Thewlis, K. M.; Yusaf, S. P. Discovery of *N*-[(2*S*)-5-(6-fluoro-3-pyridinyl)-2,3-dihydro-1*H*-inden-2-yl]-2-

propanesulfonamide, a novel clinical AMPA receptor positive modulator. *J. Med. Chem.* **2010,** *53*, 5801-5812.

20. (a) Fleming, J. J.; England, P. M. Developing a complete pharmacology for AMPA receptors: a perspective on subtype-selective ligands. *Bioorg. Med. Chem.* **2010,** *18*, 1381-1387. (b) Harms, J. E.; Benveniste, M.; Maclean, J. K. F.; Partin, K. M.; Jamieson, C. Functional analysis of a novel allosteric modulator of AMPA receptors derived from a structure-based drug design strategy. *Neuropharmacology* **2013,** *64*, 45-52.

21. Shaffer, C. L.; Scialis, R. J.; Rong, H.; Obach, R. S. Using Simcyp to project human oral pharmacokinetic variability in early drug research to mitigate mechanism-based adverse events. *Biopharm. Drug Dispos.* **2012,** *33*, 72-84.

22. Shaffer, C. L.; Scialis, R. J.; Lotarski, S.; Bryce, D. K.; Liu, J.; Majchrzak, M. J.; Christoffersen, C.; Hoffmann, W. E.; Campbell, B.; Hurst, R. S.; McLean, S.; Ganong, A. H.; Hajos, M.; Seymour, P. A.; Menniti, F. S.; Schmidt, C. J. Defining the mechanism-mediated exposure-response continuum of a novel AMPA receptor potentiator (Abstract). *Soc. Neurosci. Abstr.* **2009**, 883.17.

23. McNeish, J.; Roach, M.; Hambor, J.; Mather, R. J.; Weibley, L.; Lazzaro, J.; Gazard, J.; Schwarz, J.; Volkmann, R.; Machacek, D.; Stice, S.; Zawadzke, L.; O'Donnell, C.; Hurst, R. High-throughput screening in embryonic stem cell-derived neurons identifies potentiators of α-amino-3-hydroxyl-5-methyl-4-isoxazolepropionate-type glutamate receptors. *J. Biol. Chem.* **2010,** *285*, 17209-17217.

24. (a) Ornstein, P. L.; Zimmerman, D. M.; Arnold, M. B.; Bleisch, T. J.; Cantrell, B.; Simon, R.; Zarrinmayeh, H.; Baker, S. R.; Gates, M.; Tizzano, J. P.; Bleakman, D. Biarylpropylsulfonamides as Novel, Potent Potentiators of 2-Amino-3-(5-methyl-3-

hydroxyisoxazol-4-yl)-propanoic Acid (AMPA) Receptors. *J. Med. Chem.* **2000,** *43*, 4354-4358. (b) Quirk, J. C.; Nisenbaum, E. S. LY404187: A novel positive allosteric modulator of AMPA receptors. *CNS Drug Rev.* **2002,** *8*, 255-282.

25. Wager, T. T.; Hou, X.; Verhoest, P. R.; Villalobos, A. Moving beyond rules: the development of a central nervous system multiparameter optimization (CNS MPO) approach to enable alignment of druglike properties. *ACS Chem. Neurosci.* **2010,** *1*, 435-449.

26. Gehlhaar, D. K.; Verkhivker, G. M.; Rejto, P. A.; Sherman, C. J.; Fogel, D. B.; Fogel, L. J.; Freer, S. T. Molecular recognition of the inhibitor AG-1343 by HIV-1 protease: conformationally flexible docking by evolutionary programming. *Chem. Biol.* **1995,** *2*, 317-324.

27. (a) Cram, D. J. Preorganization - from solvents to spherands. *Angew. Chem.* **1986,** *25*, 1039-1134. (b) Cram, D. J. The design of molecular hosts, guests, and their complexes (Nobel lecture). *Angew. Chem.* **1988,** *27*, 1009-1112. (c) Lehn, J.-M. Supramolecular chemistry - scope and perspectives. Molecules, supermolecules, and molecular devices (Nobel lecture). *Angew. Chem.* **1988,** *27*, 89-112. (d) Lehn, J.-M. Perspectives in supramolecular chemistry - from molecular recognition towards molecular information processing and self-organization. *Angew. Chem.* **1990,** *29*, 1304-1319. (e) Pedersen, C. J. The discovery of crown ethers (Nobel lecture). *Angew. Chem.* **1988,** *27*, 1021-1027.

28. (a) Wolfe, S. The gauche effect. Some stereochemical consequences of adjacent electron pairs and polar bonds. *Accounts Chem. Res.* **1972,** *5*, 102-111. (b) Juaristi, E. The attractive and repulsive gauche effects. *J. Chem. Educ.* **1979,** *56*, 438-441. (c) Burke, S. D.; O'Donnell, C. J.; Porter, W. J.; Song, Y. Cyclic hydropyran oligolides as preorganized ligand arrays: cumulative effects of structural elements on shape and cation binding. *J. Am. Chem. Soc.* **1995,** *117*, 12649-12650.

29. Thewlis, K. M.; Aldegheri, L.; Harries, M. H.; Mookherjee, C.; Oliosi, B.; Ward, S. E. N-Substituted pyrollidones and tetrahydrofurans as novel AMPAR positive modulators. *Bioorg. Med. Chem. Lett.* **2010,** *20*, 7116-7119.

30. Wager, T. T.; Villalobos, A.; Verhoest, P. R.; Hou, X. J.; Shaffer, C. L. Strategies to optimize the brain availability of central nervous system drug candidates. *Expert Opin. Drug Discov.* **2011,** *6*, 371-381.

31. Hughes, J. D.; Blagg, J.; Price, D. A.; Bailey, S.; DeCrescenzo, G. A.; Devraj, R. V.; Ellsworth, E.; Fobian, Y. M.; Gibbs, M. E.; Gilles, R. W.; Greene, N.; Huang, E.; Krieger-Burke, T.; Loesel, J.; Wager, T. T.; Whiteley, L.; Zhang, Y. Physiochemical drug properties associated with in vivo toxicological outcomes. *Bioorg. Med. Chem. Lett.* **2008,** *18*, 4872-4875.

32. Jin, R.; Clark, S.; Weeks, A. M.; Dudman, J. T.; Gouaux, E.; Partin, K. M. Mechanism of Positive Allosteric Modulators Acting on AMPA Receptors. *J. Neurosci.* **2005,** *25*, 9027-9036.

33. Olney, J. W.; Newcomer, J. W.; Farber, N. B. NMDA receptor hypofunction model of schizophrenia. *J. Psychiatr. Res.* **1999,** *33*, 523-533.

34. (a) Strick, C. A.; Li, C.; Scott, L.; Harvey, B.; Hajos, M.; Steyn, S. J.; Piotrowski, M. A.; James, L. C.; Downs, J. T.; Rago, B.; Becker, S. L.; El-Kattan, A.; Xu, Y.; Ganong, A. H.; Tingley, F. D.; Ramirez, A. D.; Seymour, P. A.; Guanowsky, V.; Majchrzak, M. J.; Fox, C. B.; Schmidt, C. J.; Duplantier, A. J. Modulation of NMDA receptor function by inhibition of D-amino acid oxidase in rodent brain. *Neuropharmacology* **2011,** *61*, 1001-1015. (b) Kozak, R.; Campbell, B. M.; Strick, C. A.; Horner, W. E.; Hoffman, W. E.; Kiss, T.; Chapin, D. S.; McGinnis, D.; Abbott, A. L.; Roberts, B. M.; Fonseca, K.; Guanowsky, V.; Young, D. A.; Seymour, P. A.; Dounay, A.; Hajos, M.; Williams, G. V.; Castner, S. A. Reduction of brain kynurenic acid improves cognitive function. *J. Neurosci.* **2014,** *34*, 10592-10602.

35. Menniti, F. S.; Buchan, A. M.; Chenard, B. L.; Critchett, D. J.; Ganong, A. H.; Guanowsky, V.; Seymour, P. A.; Welch, W. M. CP-465,022, a selective noncompetitive AMPA receptor antagonist, blocks AMPA receptors but is not neuroprotective in vivo. *Stroke* **2003,** *34*, 171-176.

36. Goldman-Rakic, P. S. Working memory dysfunction in schizophrenia. *J. Neuropsychiatry Clin. Neurosci.* **1994,** *6*, 348-357.

37. (a) Tamminga, C. A.; Stan, A. D.; Wagner, A. D. The hippocampal formation in schizophrenia. *Am. J. Psychiatr.* **2010,** *167*, 1178-1193. (b) Lisman, J., Excitation, inhibition, local oscillations, or large-scale loops: what causes the symptoms of schizophrenia? *Curr. Opin. Neurobiol.* **2012,** *22*, 537-544.

38. (a) Lidow, M. S.; Williams, G. V.; Goldman-Rakic, P. S. The cerebral cortex: a case for a common site of action of antipsychotics. *TiPS* **1998,** *19*, 136-140. (b) Calabrese, E. J. Alzheimer's disease drugs: an application of the hormetic dose-response model. *Crit. Rev. Toxicol.* **2008,** *38*, 419-451. (c) Hutson, P. H.; Finger, E. N.; Magliaro, B. C.; Smith, S. M.; Converso, A.; Sanderson, P. E.; Mullins, D.; Hyde, L. A.; Eschle, B. K.; Turnbull, Z.; Sloan, H.; Guzzi, M.; Zhang, X.; Wang, A.; Rindgen, D.; Mazzola, R.; Vivian, J. A.; Eddins, D.; Uslaner, J. M.; Bednar, R.; Gambone, C.; Le-Mair, W.; Marino, M. J.; Sachs, N.; Xu, G.; Parmentier-Batteur, S. The selective phosphodiesterase 9 (PDE9) inhibitor PF-04447943 (6-[3*S*,4*S*)-4-methyl-1-(pyrimidin-2-ylmethyl)pyrrolidin-3-yl]-1-(tetrahydro-2*H*-pyran-4-yl)-1,5-dihydro-4*H*-pyrazolo[3,4-*d*]pyrimidin-4-one) enhances synaptic plasticity and cognitive function in rodents. *Neuropharmacology* **2011,** *61*, 665-676.

39. Zasadny, K.; Callahan, M. J.; Kuszpit, K.; Chen, L.; Skaddan, M.; Brown-Proctor, C.; Harris, R.; Zhu, A.; Shaffer, C. L.; Scialis, R. J. FDG-PET imaging provides insights into

efficacy and safety for an AMPA receptor potentiator (Abstract). *World Mol. Imaging Soc. Abstr.* **2009**, 909.

40. Williams, G. V.; Roberts, B. M.; Holden, D. E.; Campbell, D. W.; Shaffer, C. L.; Scialis, R. J.; Seymour, P. A.; Menniti, F. S.; Schmidt, C. J.; Sandiego, C. M.; Carson, R. E.; Castner, S. A. Cerebral metabolic correlates of ketamine-induced cognitive deficits and their reversal by a positive allosteric modulator of the AMPA receptor: a functional imaging study in the nonhuman primate using FDG-PET (Abstract). *Soc. Neurosci. Abstr.* **2009**, 883.17.

41. Williams, G. V.; Abbott, A. L.; Campbell, D. W.; Honey, G. D.; Shaffer, C. L.; Osgood, S. M.; Seymour, P. A.; Schmidt, C. J.; Sandiego, C. M.; Carson, R. E.; Castner, S. A. Investigation of the dose-dependent effect of the AMPA potentiator PF-04958242 on cerebral glucose metabolism: significance for development of a PET biomarker for efficacy or procognitive agents in schizophrenia (Abstract). *Soc. Neurosci. Abstr.* **2011**, 899.07.

42. Jamei, M.; Marciniak, S.; Feng, K.; Barnett, A.; Tucker, G.; Rostami-Hodjegan, A. The Simcyp population-based ADME simulator. *Expert Opin. Drug Metab. Toxicol.* **2009,** *5*, 211-223.

43. Bednar, M. M.; DeMartinis, N.; Banerjee, A.; Bowditch, S.; Gaudreault, F.; Zumpano, L.; Lin, F. R. The safety and efficacy of PF-04958242 in age-related sensorineural hearing loss: a randomized, double-blind, placebo-controlled, single-dose, crossover study. *JAMA Otolaryngol. Head Neck Surg.* **2015,** *in press*.

44. Resources, I. o. L. A., Guide for the Care and Use of Laboratory Animals. 7th ed.; Commission on Life Sciences, N. R. C., Ed. Washington, D.C., 1996.

45. Ryder, J. W.; Falcone, J. F.; Manro, J. R.; Svensson, K. A.; Merchant, K. M. Pharmacological Characterization of cGMP Regulation by the Biarylpropylsulfonamide Class of

Positive, Allosteric Modulators of α-Amino-3-hydroxy-5-methyl-4-isoxazolepropionic Acid Receptors. *J. Pharmacol. Exp. Ther.* **2006,** *319*, 293-298.

46. Dunham, N. W.; Miya, T. S. A note on a simple apparatus for detecting neurological deficit in rats and mice. *J. Am. Pharm. Assoc.* **1957,** *XLVI*, 208-209.

47. Kiss, T.; Hoffman, W. E.; Scott, L.; Kawabe, T. T.; Milici, A. J.; Nilsen, E. A.; Hajós, M. Role of thalamic projection in NMDA receptor-induced disruption of cortical slow oscillation and short-term plasticity. *Front. Psychiatry* **2011,** *2*, 1-12.

48. Cox, R. W. AFNI: software for analysis and visualization of functional magnetic resonance neuroimages. *Comput. Biomed. Res.* **1996,** *29*, 162-173.

49. (a) Obach, R. S.; Baxter, J. G.; Liston, T. E.; Silber, B. M.; Jones, B. C.; MacIntyre, F.; Rance, D. J.; Wastall, P. The Prediction of Human Pharmacokinetic Parameters from Preclinical and *In Vitro* Metabolism Data. *J. Pharmacol. Exp. Ther.* **1997,** *283*, 46-58. (b) Brown, H. S.; Griffin, M.; Houston, J. B. Evaluation of cryopreserved human hepatocytes as an alternative in vitro system to microsomes for the prediction of metabolic clearance. *Drug Metab. Dispos.* **2007,** *35*, 293-301.

TABLES

Table 1. AMPAR Functional activity and select physicochemical properties of carbon linker ether analogs **6–9**

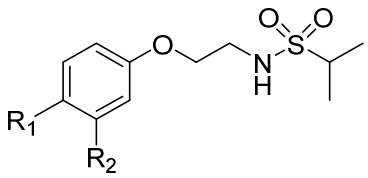

Compound	R_1	R_2	EC_{50} (nM)[a]	E_{max} (%)[b]	MW (amu)	clogP	TPSA (Å^2)
5	NA	NA	3400	132	342	3.79	78.0
6	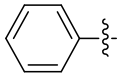	H	2440	32	319	4.03	63.8
7	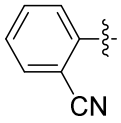	H	7350	218	344	3.53	87.6
8	H	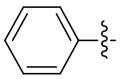	>31600	15	319	4.03	63.8
9	H	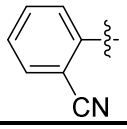	>31600	33	344	3.53	87.6

NA, not applicable; [a]Functional potency (EC_{50}; geometric mean, N≥3) in mouse ES cell-derived neurons as assessed by measuring effects induced by *S*-AMPA (100 μM) alone and following potentiator (up to 32 μM) pretreatment using fluorometric imaging plate reading (FLIPR); [b]Functional efficacy (E_{max}; arithmetic mean, N≥3) in the aforementioned mouse ES cell-derived neurons assay relative to the average response to *S*-AMPA (100 μM) in the presence of cyclothiazide (32 μM), which was defined as 100%.

Table 2. SAR of tetrahydrofuran ethers with a select aryl or heteroaryl distal aromatic ring

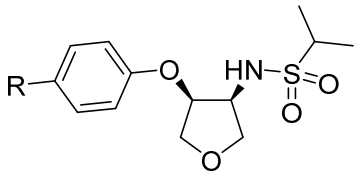

Compound	*	R	EC_{50} (nM)[a]	E_{max} (%)[b]	K_i (nM)[c]	MW (amu)	clogP	TPSA (Å^2)	HLM CL_{int} (mL/min/kg)[d]	$P_{app,A\rightarrow B}$ ($\times10^{-6}$ cm/s)[e]	MDR1 BA/AB[f]
17	(±)	Ph	2480	125	ND	361	4.13	64.6	29.5	ND	ND
18	(±)	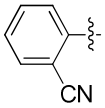	21.9	154	ND	386	3.63	88.4	54.2	21.3	1.36
19	*3S,4S*	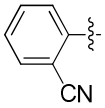	21.7	143	7.7	386	3.63	88.4	138	32.3	1.39
20	*3R,4R*	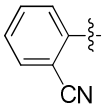	17500	126	ND	386	3.63	88.4	47.4	23.3	1.65
21	*3S,4S*	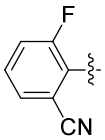	14.1	85	17.2	404	3.78	88.4	89.1	20.6	1.04
22	*3S,4S*	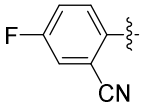	<10.0	190	11.1	404	3.78	88.4	39.3	19.6	1.32
23	(±)	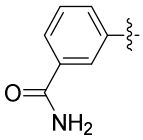	1110	102	ND	404	2.69	107.7	<9.9	17.4	7.84
24	(±)	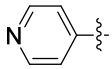	626	161	ND	362	2.73	77.5	<8.0	ND	0.90
25	(±)	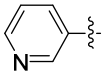	1162	161	78.9	362	2.73	77.5	<8.0	ND	1.24
26	(±)	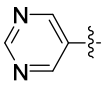	1086	110	ND	363	1.80	90.4	20.8	26.0	1.12
3	*3S,4S*	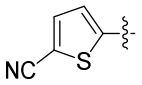	310	110	170	392	3.54	88.4	<8.0	19.3	1.05
27	*3S,4S*	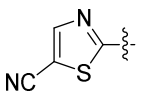	274	135	258	393	2.38	101.3	13.5	24.9	1.11
28	*3S,4S*	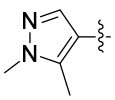	157	67	270	379	2.27	82.4	<8.0	21.7	1.32

ND, not determined; [a]Functional potency (EC_{50}; geometric mean, N≥3) in mouse ES cell-derived neurons as assessed by measuring effects induced by *S*-AMPA (100 μM) alone and following potentiator (up to 32 μM) pretreatment using fluorometric imaging plate reading (FLIPR); [b]Functional efficacy (E_{max}; arithmetic mean, N≥3) in the aforementioned mouse ES cell-derived neurons assay relative to the average response to *S*-AMPA (100 μM) in the presence of cyclothiazide (32 μM), which was defined as 100%; [c]K_i (geometric mean, N≥3) determined by displacement studies using [^{3}H]PF-04725379 in rat cortical tissue; [d]Human liver microsomes-derived intrinsic clearance; [e]RRCK cells, isolated from Madin-Darby canine kidney cells and having low transporter activity, were used to estimate absorptive apparent permeability ($P_{app,A\rightarrow B}$) of a potentiator (1 μM); [f]The ratio of secretory apparent permeability ($P_{app,B\rightarrow A}$) to $P_{app,A\rightarrow B}$ of a potentiator (1 μM) across contiguous monolayers from human multidrug resistance protein-1-transfected MDCK cells (MDR1-MDCK).

Table 3. Summary of the primary in vitro pharmacology and interspecies exposure-response continuum for **3**

Assay	Concentration or $C_{b,u}$ (nM)
In vitro[a]	
Rat cortical tissue K_i	170
Rat primary cortical neurons EC_{50}	43 ± 10
mES cell-derived neurons EC_{50} (Efficacy, %)	310 (110 ± 4%)
hGluA2i EC_{50} (Efficacy, %)	24 (124 ± 11%)
hGluA2o EC_{50} (Efficacy, %)	880 (108 ± 5%)
In vivo	
Rotarod	10.8
cGMP	6.7
PPF[b]	0.23 / 0.18
RAM	0.029 – 0.29

[a]Geometric means for K_i and EC_{50}, arithmetic means ± SEM for percent efficacy, N≥3 for each assay; [b]$C_{b,u}$ were determined by the Spearman-Karber-determined ED_{50} (0.003 mg/kg, IV) from the cumulative-dose study or the PK/PD model-derived value that was able to reverse 50% of the MK-801-induced PPF disruption in the single-dose (0.01 mg/kg, IV) time course study, respectively.

Table 4. Mean pharmacokinetic parameters of **3** in rats, dogs and nonhuman primates (NHP)

Parameter	Species[a]		
	Rat	Dog	NHP
$f_{u,p}$	0.048	0.070	0.110
$f_{u,b}$	0.019	ND	ND
$C_{b,u}$:$C_{p,u}$	0.59[b]	ND	ND
CL_p (mL/min/kg)	169 / NA	11.2[c]	NA
V (L/kg)	3.6 / NA	6.0[c]	NA
$t_{1/2}$ (h)	0.31 / 0.84	6.21	12.3
C_{max} (ng/mL)	NA / 134	23.9	6.87
T_{max} (h)	NA / 0.25	0.79	4.0
$AUC_{0-\infty}$ (ng•h/mL)	20.1 / 175	158	149
F (%)	58	ND	ND
$f_{u,LM}$	0.42	0.46	0.44
B/P[d]	0.84	0.87	0.90
LM CL_H (mL/min/kg)[e]	40.2 / 63.6	1.5 / 7.4	10.2 / 22.8
IM $CL_{int,app}$ (μL/min/mg)[f]	<15	<22	<29

ND, not determined; NA, not applicable; [a]In vivo pharmacokinetic parameters were determined using doses of: 0.2 mg/kg, IV (N=2) / 3.0 mg/kg, PO (N=3) for rats; 0.1 mg/kg, PO (N=6) for dogs; and, 0.032 mg/kg, SC (N=2) for NHP; [b]$AUC_{0-Tlast}$-derived ratio of unbound brain compound concentration-to-unbound plasma compound concentration ($C_{b,u}$:$C_{p,u}$) determined in a rat neuropharmacokinetics study (1 mg/kg, SC; N=2/time point); [c]Apparent value; [d]Blood-to-plasma concentration ratio; [e]Liver microsomes-derived hepatic blood clearance (LM CL_H) using the well-stirred model with/without binding factors; [f]Intestinal microsomes-derived apparent intrinsic clearance (IM $CL_{int,app}$) without binding factors.

Table 5. Projected human pharmacokinetic parameters and human binding factors for **3**

Parameter	**3**
C_{eff} (ng/mL)	2.4
CL_p (mL/min/kg)	3.12
F_H	0.81
$F_a \bullet F_g$	1.00[a]
F (%)	81
V_{ss} (L/kg)	0.63[b]
$t_{1/2}$ (h)	3.0
Dose (mg)	0.3 BID[c]
$f_{u,p}$	0.079
$f_{u,HLM}$	0.52
B/P[d]	0.82
HLM CL_H (mL/min/kg)[e]	0.8 / 3.8
HHeps CL_H (mL/min/kg)[e]	ND / 7.1
HIM $CL_{int,app}$ (μL/min/mg)[f]	<15
rhCYP $CL_{int,app}$ (μL/min/pmol)[f]	CYP3A4 (0.472), CYP2C19 (0.061)

ND, not determined; [a]Calculated from rat IV / PO pharmacokinetics studies; [b]In silico-derived value; [c]Projected using $C_{ss,av} = (CL_p \bullet \tau \bullet C_{eff})/F$ and assuming a 70 kg subject; [d]Blood-to-plasma concentration ratio; [e]Human liver microsomes (HLM)- or human hepatocytes (HHeps)-derived hepatic blood clearance (CL_H) using the well-stirred model with/without binding factors; [f]Human intestinal microsomes- or recombinant human CYP (rhCYP)-derived apparent intrinsic clearance ($CL_{int,app}$) without binding factors.

FIGURE LEGENDS

Figure 1. Representative compounds of the tetrahydropyran (**1**), dihydroisoxazole (**2** and **4**), tetrahydrofuran ether (**3**) and biarylpropylsulfonamide (**5**) structural classes of AMPAR potentiators.

Figure 2. A visualization of the design hypotheses explored to discover a unique chemotype from the biarylpropylsulfonamide structural class of AMPAR potentiators (exemplified by **5**).

Figure 3. A model of **7** (cyan) docked onto the X-ray co-crystal structure of **5** (magenta) in the symmetrical binding pocket of the human GluA2o LBD. Only one binding pose of symmetric poses for each compound is shown for clarity. The sulfonamide of **5** forms a hydrogen bond with the backbone carbonyl oxygen of Pro-494; assuming an identical interaction, the sulfonamide of **7** was overlaid onto that of **5**.

Figure 4. A visualization of the heterocycle design hypothesis from **7**. Panel A: A Newman projection of the structural conformation of the energy-minimized model of **7** projected to bind to the GluA2o LBD. Panel B: The design hypotheses based on the ring-construction strategy to constrain the GluA2o LBD-bound conformation of **7**.

Figure 5. The X-ray co-crystal structure of **3** in the symmetrical binding pocket of the human GluA2o LBD. For each molecule, only one binding pose is shown for clarity. The sulfonamide

of **3** interacts with Pro-494 when its 2-cyano moiety accesses a flip isoform-selective pocket. The flip vs. flop GluA2 isoforms are differentiated by a Ser vs. Asn, respectively, at amino acid 754.

Figure 6. Compound **3** dose-dependently increased CD-1 mouse cerebellum cGMP (A) and decreased fall latency in C57BL/6J mice traversing an accelerating rotarod (B). For both assays, single doses were administered subcutaneously with a 0.5 h pretreatment time; for each dose the projected mean $C_{b,u}$ at 0.5 h after administration of **3** is shown within brackets. The data are expressed as the mean ± SEM with N=5–6/dose (cGMP) or N=12/dose (rotarod). **P* <0.05 (one-way ANOVA followed by post-hoc Dunnett's *t* test).

Figure 7. In rats, **3** reversed the MK-801-mediated reduction in PPF after cumulative (A) or a single (B; 0.01 mg/kg) intravenous dose(s). Each column represents PPF values (mean ± SEM, N=3–5) collected over a 10-min period following administration of **3**, and the projected mean $C_{b,u}$ for each period is shown within brackets. Panel A: **P* <0.01 vs. vehicle-vehicle condition, $^{\#}P$ <0.01 vs. MK-801-vehicle condition (two-tailed Student's *t* test). Panel B: **P* <0.05 vs. pre-MK-801-administration (-10 min period), $^{\#}P$ <0.05 vs. post-MK-801/pre-**3**-administration (0 min period) (two-tailed Student's *t* test); arrows designate compound administration; the mean onset of the **3**-mediated effect was 8±3 min; and, **3** reversed the MK-801-disruption through 50 min post-dose.

Figure 8. Compound **3** attenuated ketamine-induced working memory disruptions in rats as determined by mean errors in a radial arm maze. Single doses were administered subcutaneously with 1 h and 0.5 h pretreatment times for **3** or the positive control (PC) and (±)-ketamine (10 mg/kg), respectively; for each dose the projected mean $C_{b,u}$ at 1 h after **3** administration is shown within brackets. The data are expressed as the mean ± SEM with N=12/dose. *, ***P* = 0.05, 0.01 vs. vehicle-ketamine condition (using a generalized linear mixed model assuming an underlying Poisson distribution followed by a Hochberg's test for multiple post hoc comparisons).

Figure 9. In rats, **3** dose-dependently affected the regional brain uptake of FDG. Panel A: Representative slices at bregma coordinates (-0.50 (top row) and -11.00 mm (bottom row)) overlaid onto rat brain histological slices with color indicating brain regions with significantly (*P* <0.05, unpaired one-tailed *t* test) increased (yellow-to-red) or decreased (blue) FDG uptake in rats (N=12/group) receiving **3** (0.027, 0.08 or 0.60 mg/kg, SC) vs. vehicle. The color bar represents both the direction and relative magnitude of the uptake change. Panel B: The number of voxels with significantly (*P* <0.05, unpaired one-tailed *t* test) increased FDG uptake in rats (N=12/group) receiving **3** (0.027, 0.08 or 0.60 mg/kg, SC) vs. vehicle within the entire volume of the cortex and cerebellum. Each voxel represents a 0.5 × 0.5 × 0.5 mm sample volume.

Figure 10. Simulated human total plasma **3** concentration-time profiles following a single (A) or multiple (B; BID for 7 d) oral dose(s) of 0.3 mg. In both plots, the mean (solid line), 5th percentile (lower dashed line) and 95th percentile (upper dashed line) plasma drug concentration-

time curves are shown to capture the intersubject pharmacokinetic variability projected by Simcyp for a virtual population of 100 healthy volunteers.

TABLE OF CONTENTS GRAPHIC

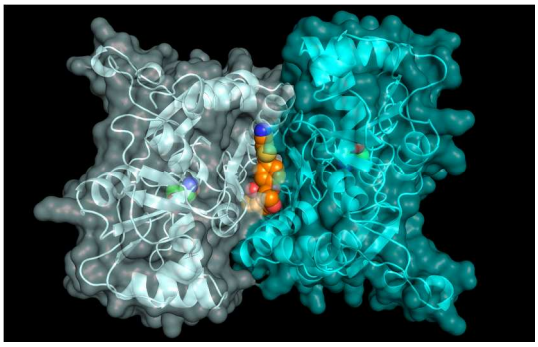

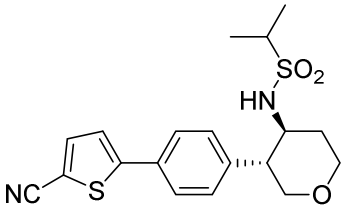

1

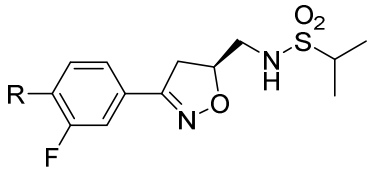

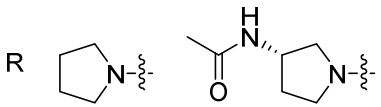

2 **4**

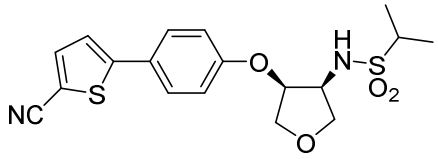

3

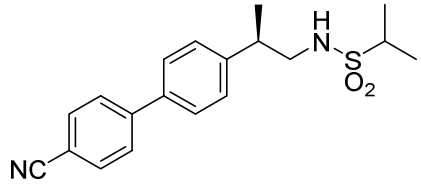

5

Figure 1

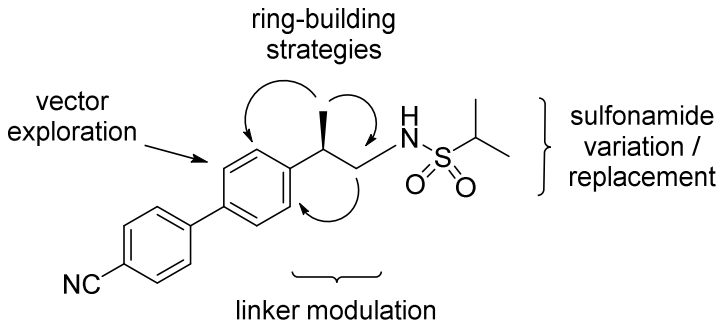
ring-building
strategies
vector
exploration
H
N
S
O
O
sulfonamide
variation /
replacement
NC
linker modulation

Figure 2

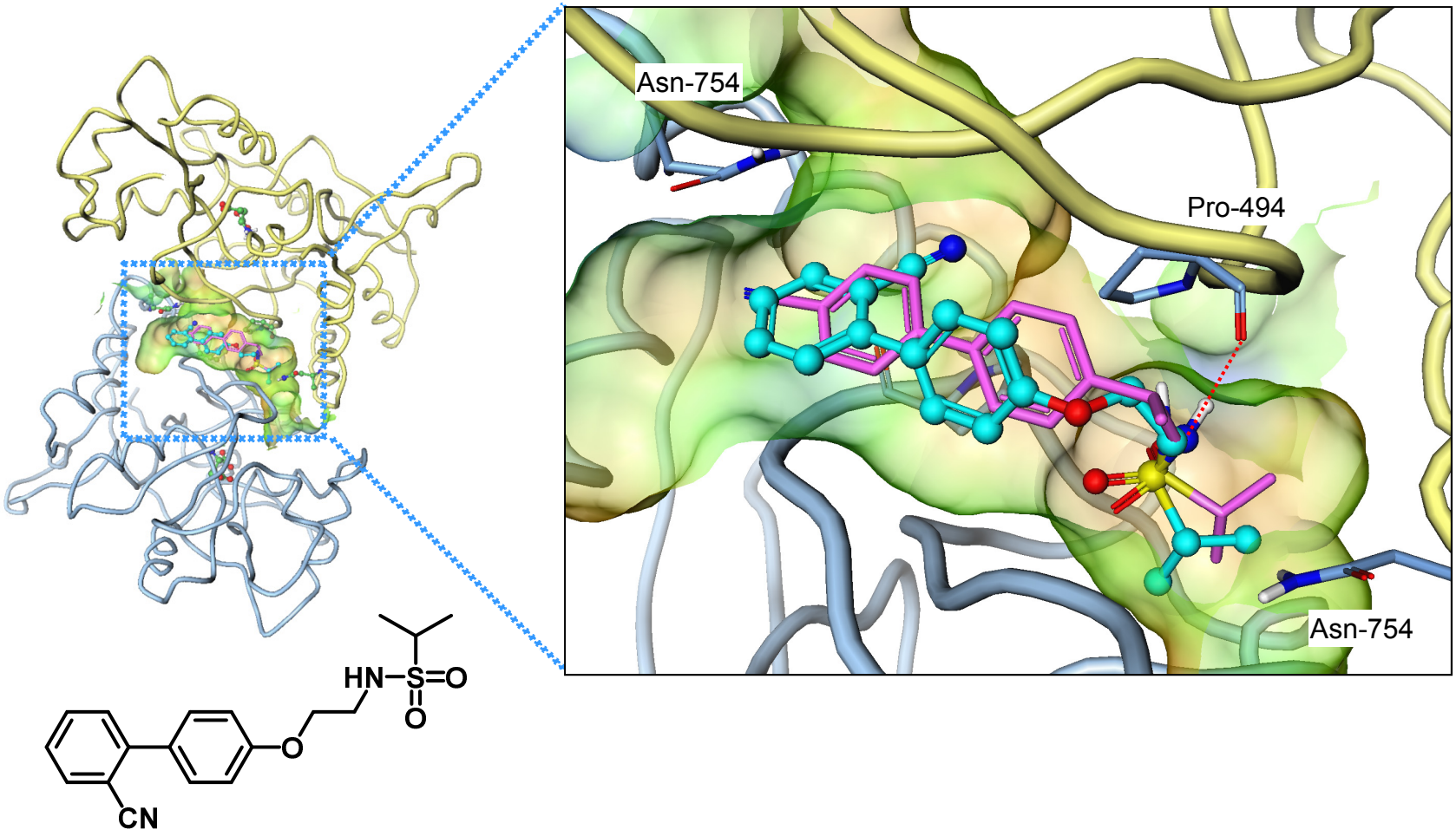

Figure 3

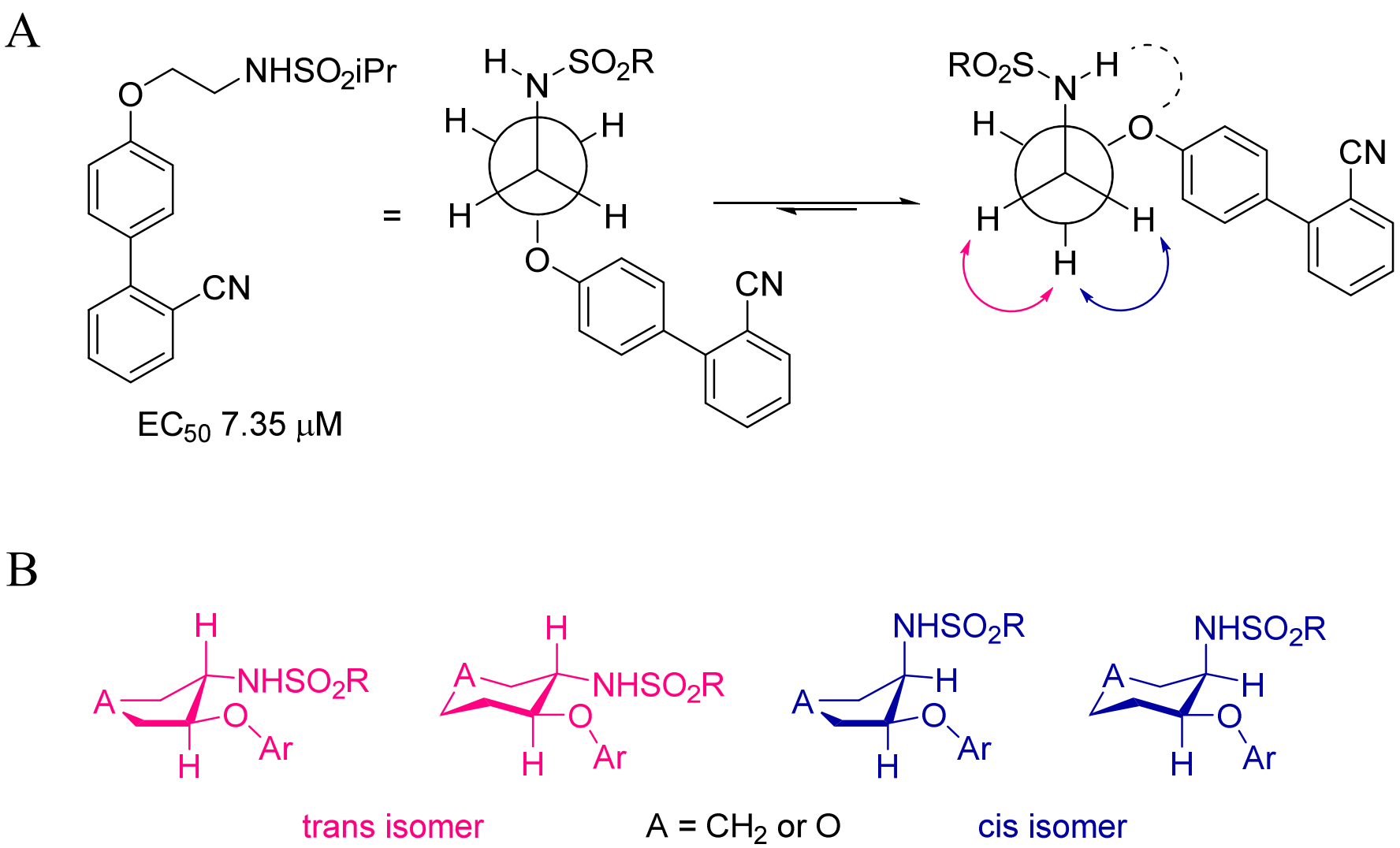

Figure 4, panels A and B

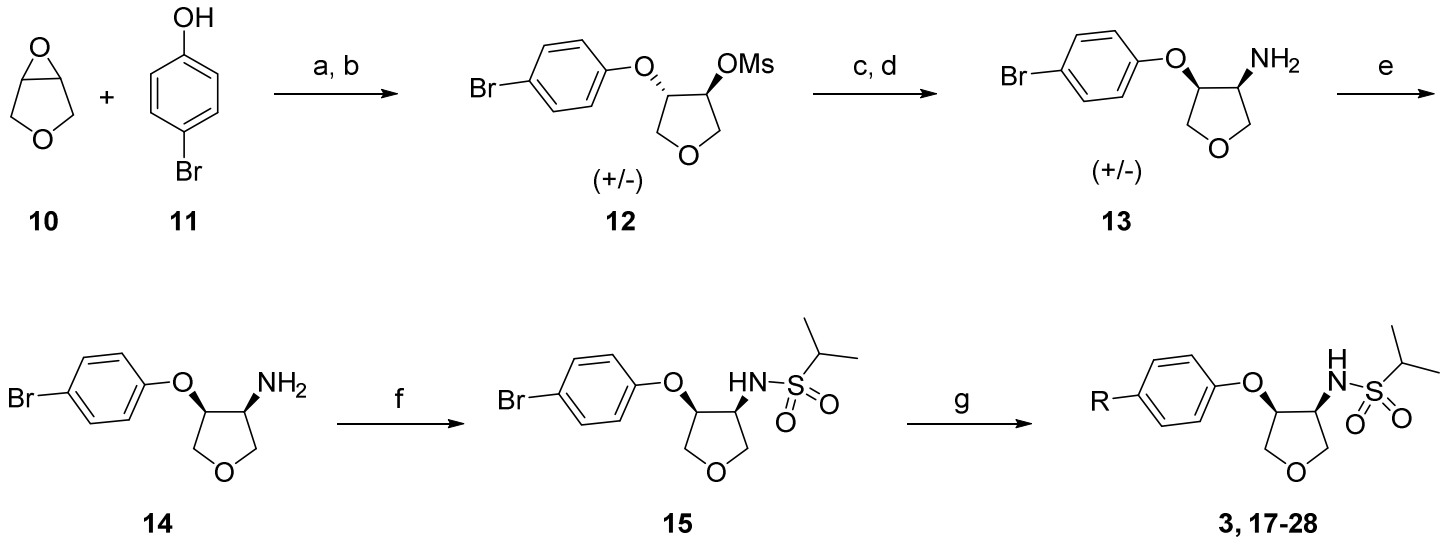

Scheme 1

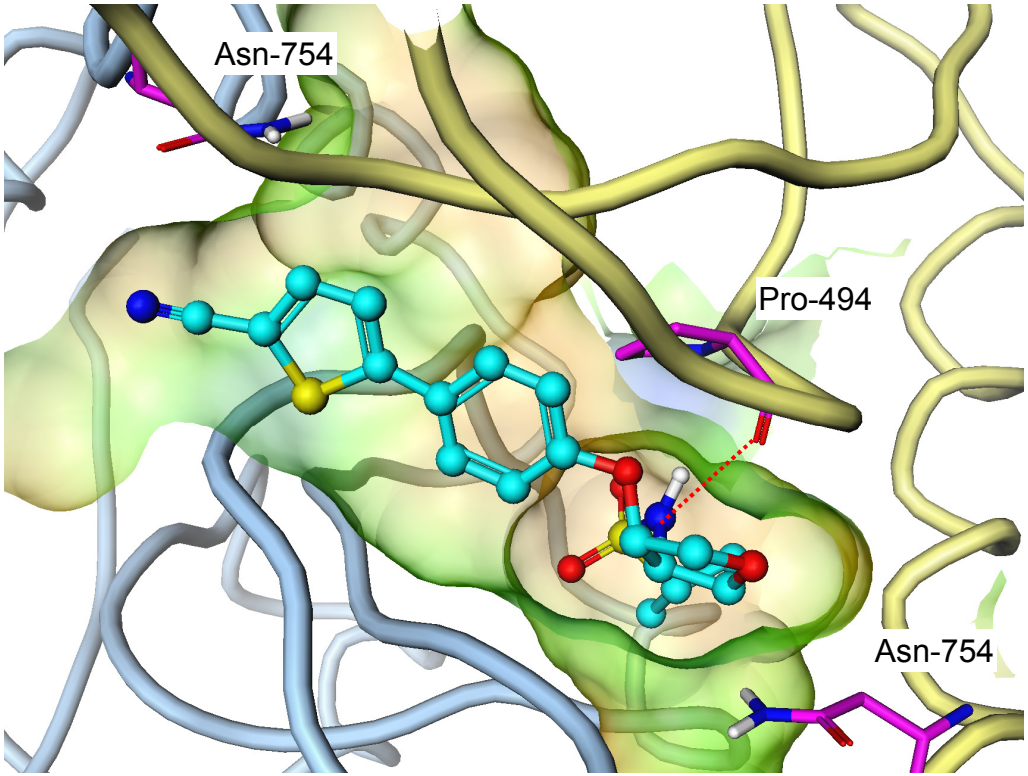

Figure 5

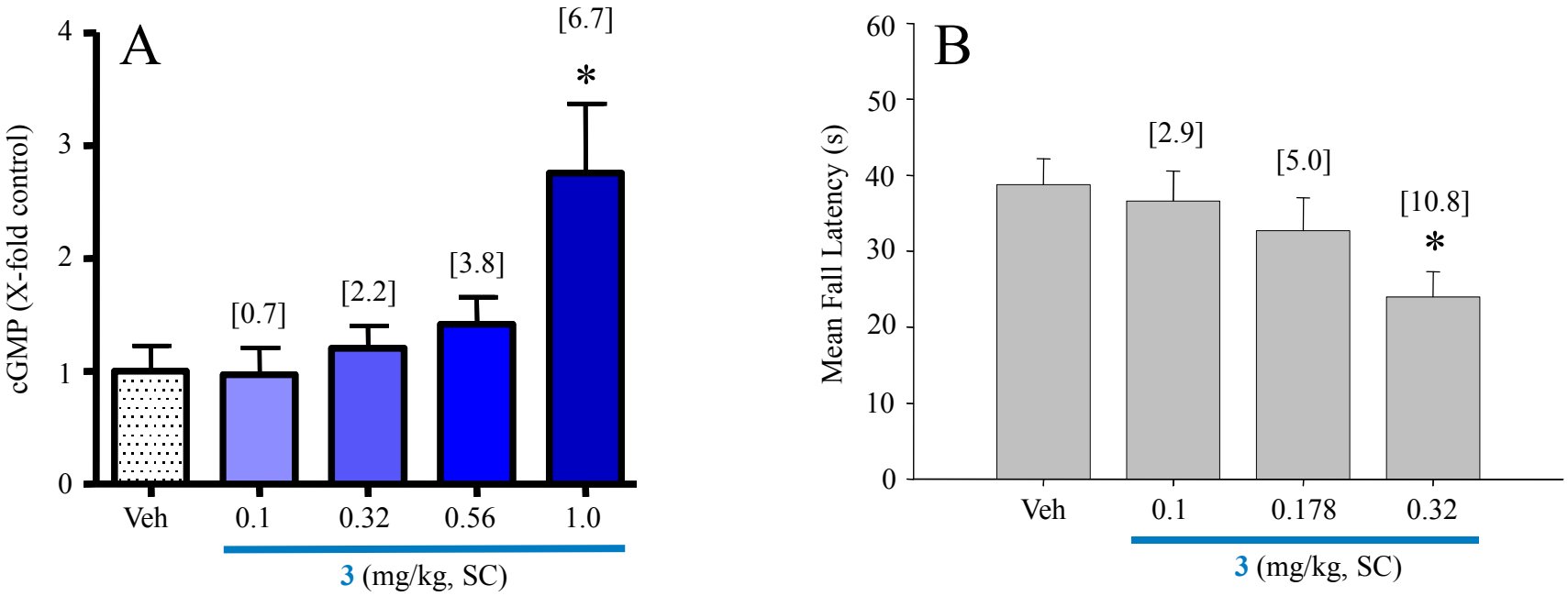

Figure 6, panels A and B

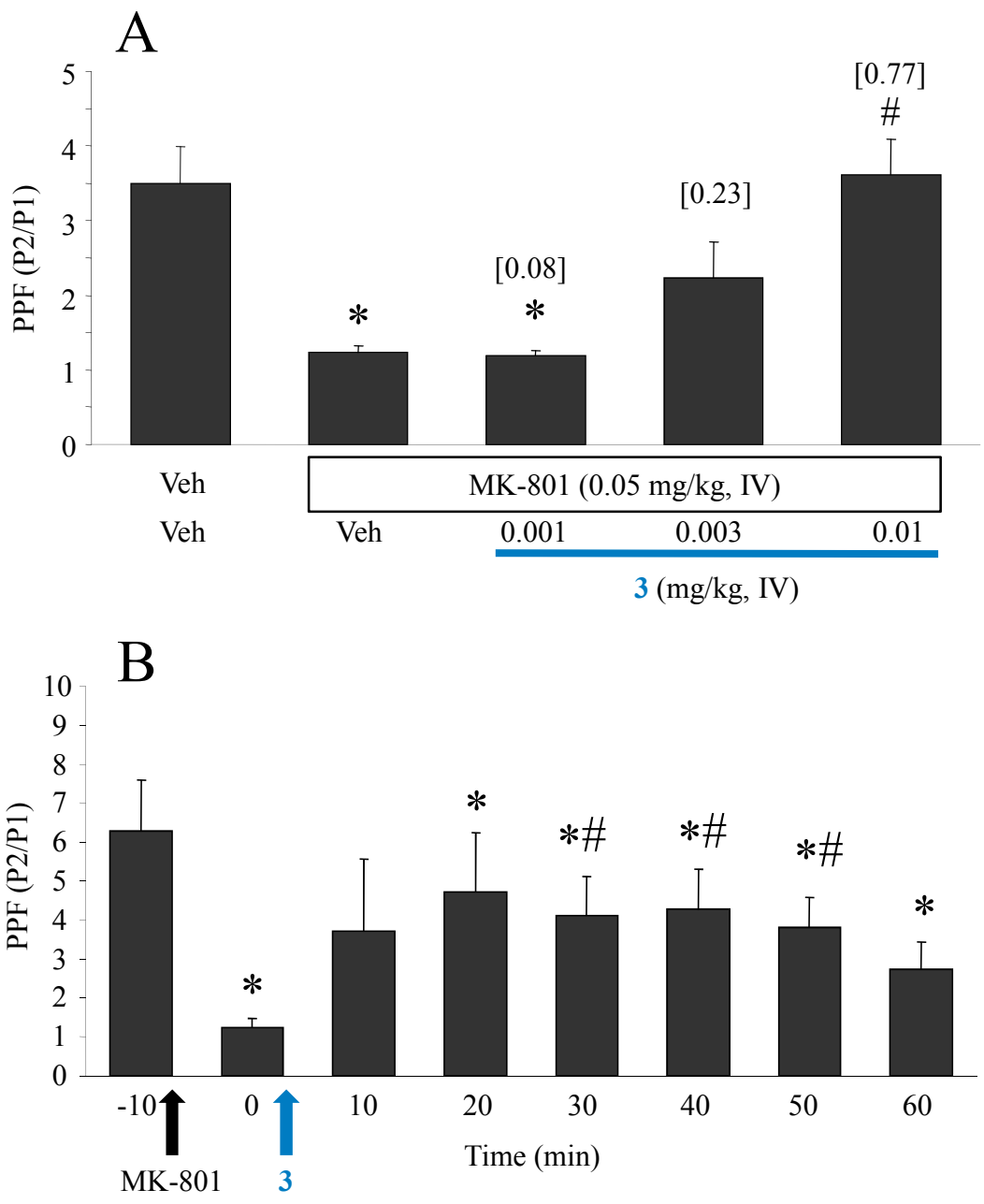

Figure 7, panels A and B

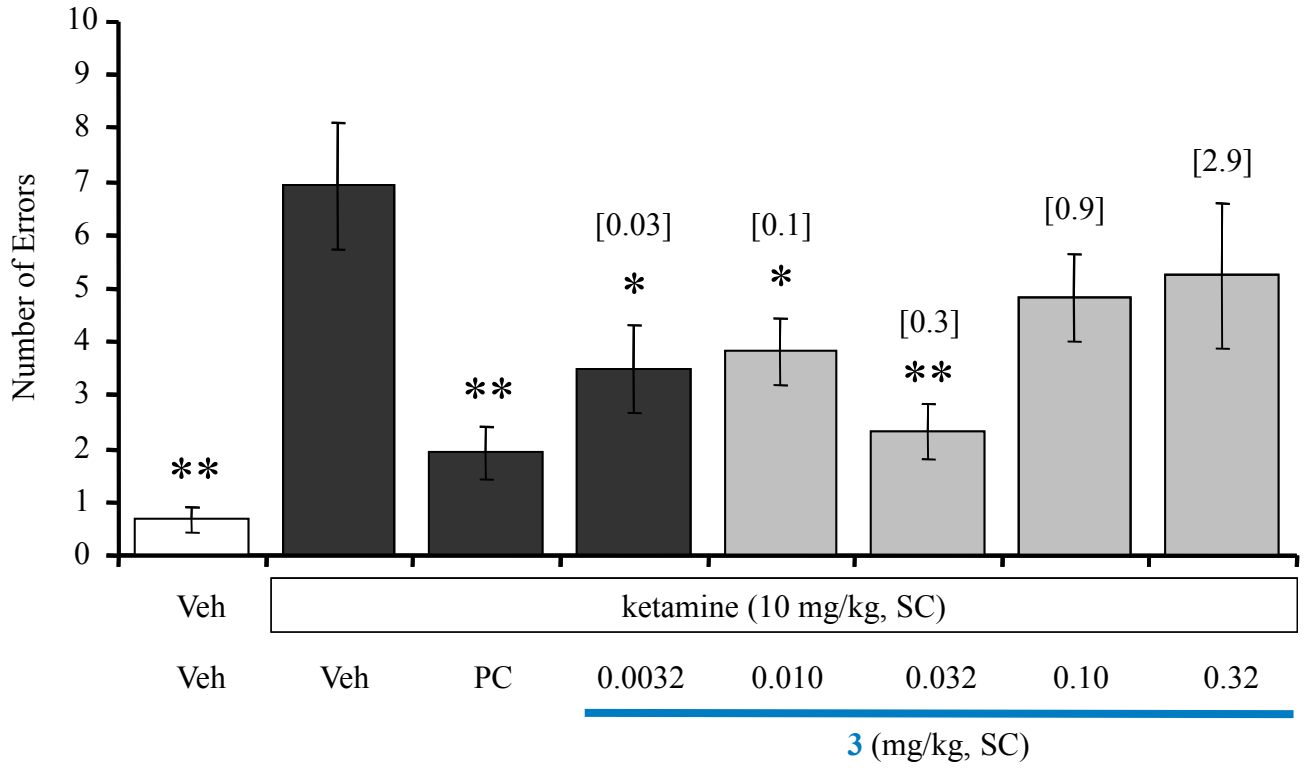
Number of Errors
10
9
8
7
6
5
4
3
2
1
0
**
**
*
*
**
[0.03]
[0.1]
[0.3]
[0.9]
[2.9]
Veh
ketamine (10 mg/kg, SC)
Veh
Veh
PC
0.0032
0.010
0.032
0.10
0.32
3 (mg/kg, SC)

Figure 8

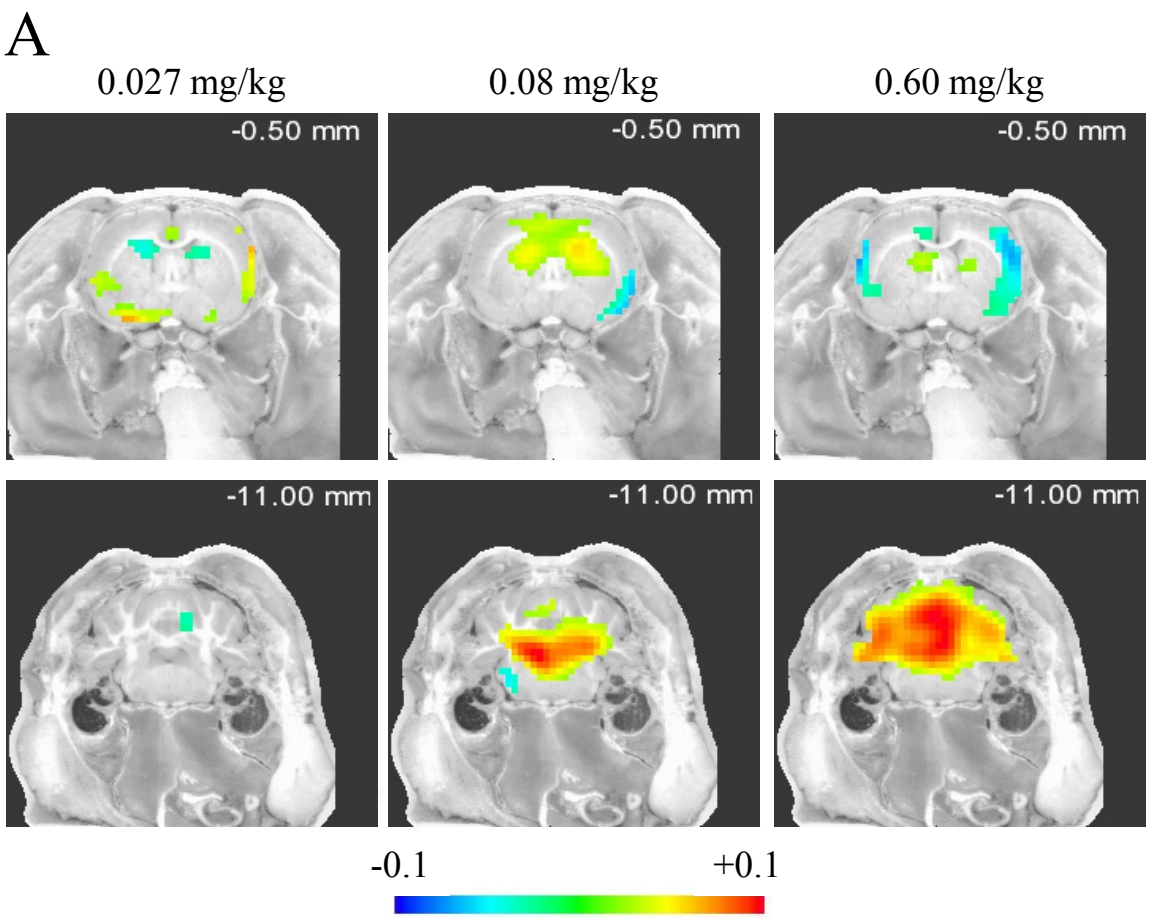

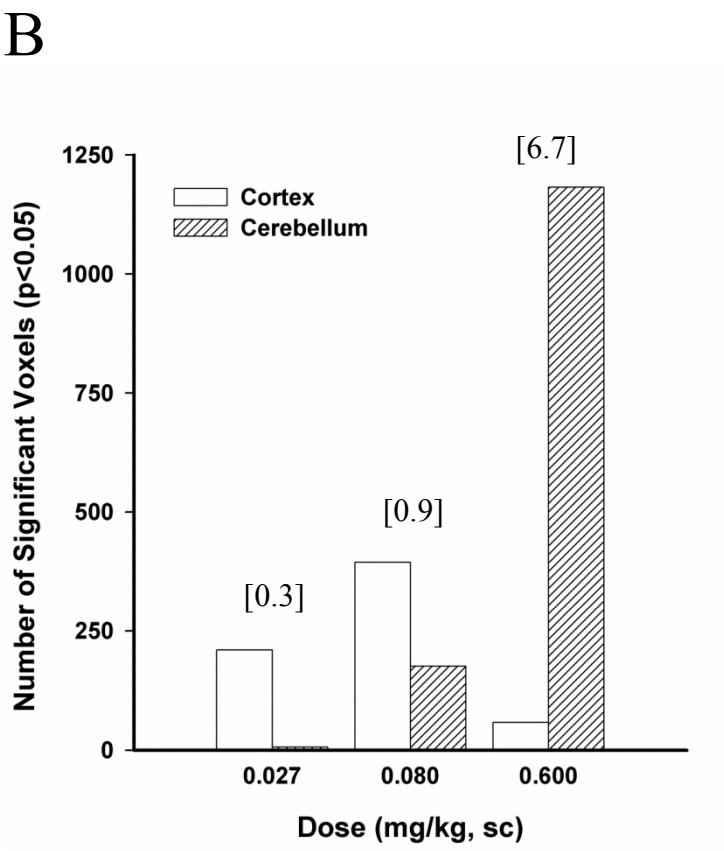

Figure 9, panels A and B

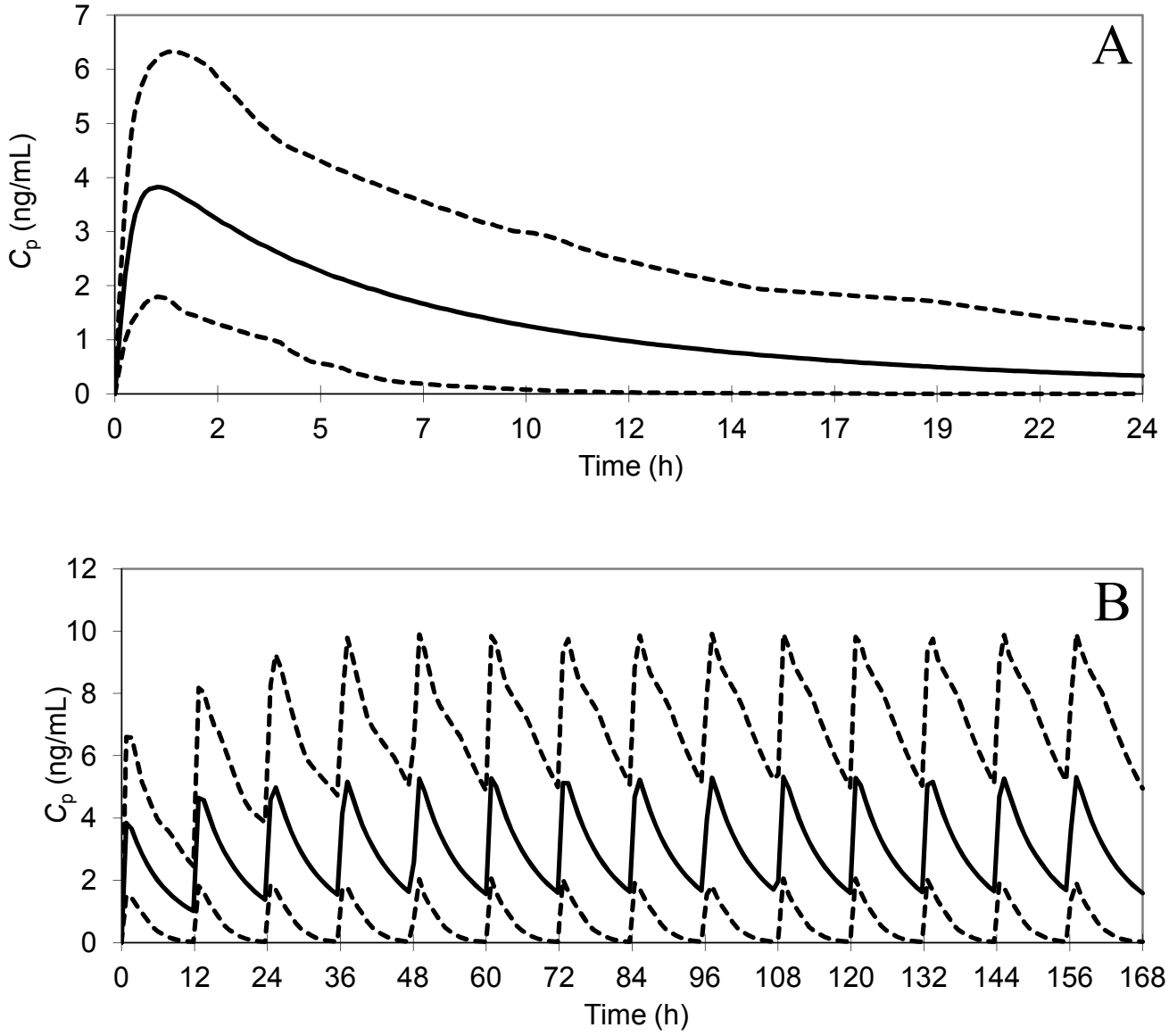

Figure 10, panels A and B